HHS Public Access

Author manuscript

Nat Commun. Author manuscript; available in PMC 2015 November 13.

Published in final edited form as:

Nat Commun. ; 6: 7114. doi:10.1038/ncomms8114.

Effector lymphocyte-induced lymph node-like vasculature enables naïve T-cell entry into tumors and enhanced anti-tumor immunity

J. David Peske[1], **Elizabeth D. Thompson**[1,2], **Lelisa Gemta**[1], **Richard A. Baylis**[1], **Yang-Xin Fu**[3], and **Victor H. Engelhard**[1,*]

[1]Department of Microbiology and Carter Immunology Center, University of Virginia, Charlottesville, VA 22901, USA

[3]Department of Pathology and Committee on Immunology, University of Chicago, Chicago, IL 60637, USA

Abstract

The presence of lymph node (LN)-like vasculature in tumors, characterized by expression of peripheral node addressin and chemokine CCL21, is correlated with T-cell infiltration and positive prognosis in breast cancer and melanoma patients. However, mechanisms controlling the development of LN-like vasculature and how it might contribute to a beneficial outcome for cancer patients are unknown. Here we demonstrate that LN-like vasculature is present in murine models of melanoma and lung carcinoma. It enables infiltration by naïve T-cells that significantly delay tumor outgrowth after intratumoral activation. Development of this vasculature is controlled by a mechanism involving effector CD8 T-cells and NK cells that secrete $LT\alpha_3$ and IFNγ. LN-like vasculature is also associated with organized aggregates of B-lymphocytes and $gp38^+$ fibroblasts that resemble tertiary lymphoid organs that develop in models of chronic inflammation. These results establish LN-like vasculature as both a consequence of and key contributor to anti-tumor immunity.

INTRODUCTION

Lymph nodes (LN) contain specialized blood vessels called high endothelial venules (HEV). HEV display peripheral node addressin (PNAd) and CCL21 and mediate entry of naïve and memory T-cells expressing the cognate ligands L-selectin and CCR7[1]. HEVs are not normally found outside lymphoid tissue but are induced at sites of chronic inflammation[2].

[*]**Corresponding Author:** Dr. Victor Engelhard, PO Box 801386, University of Virginia, Charlottesville, VA 22908, Phone: 434-924-2423 Fax: 434-924-1221, vhe@virginia.edu.

[2]Current: Department of Pathology, Johns Hopkins School of Medicine, Baltimore, MD 21287, USA

AUTHOR CONTRIBUTIONS:

Conceived and designed the experiments: J.D.P., E.D.T, and V.H.E.; Performed the experiments: J.D.P., E.D.T., L.G., R.A.B.; Analyzed the data: J.D.P., E.D.T., V.H.E.; Contributed reagents/materials/analysis tools: Y.X.F. Wrote the paper: J.D.P., V.H.E.

COMPETING FINANCIAL INTERESTS STATEMENT:

The authors have no conflicting financial interests.

They have recently been detected in human tumors and associated with a positive prognosis[3–6]. This suggests that PNAd and CCL21 on tumor vasculature are important elements of immunological tumor control, but the mechanisms inducing their expression and their function in supporting anti-tumor immunity are unknown.

In peripheral LN, HEV morphology and adhesion molecule expression are maintained by dendritic cells (DC) that express lymphotoxin (LT) $\alpha_1\beta_2$, which acts via the LTβ receptor (LTβR) on blood endothelial cells[7,8]. In inflamed non-lymphoid tissues, PNAd and CCL21 expression is often associated with the development of organized structures resembling LN termed tertiary lymphoid organs (TLO). Control of PNAd in TLO is thought to be similar to control in LN. Inhibiting LTβR signaling blocks PNAd expression in many TLO models[9–12], and DCs regulate the presence of PNAd$^+$ vasculature and associated TLO in inflamed lungs[13,14]. PNAd$^+$ vasculature can be induced by transgenic expression of LTα and LTβ in the pancreas and kidney[15,16], or by transgenic expression of CCL21 in the pancreas and thyroid via a LTβR-dependent pathway[17,18]. Similarly, transgenic expression of LTα or CCL21 in tumors leads to induction of PNAd$^+$ vasculature[19–21]. However, these transgenic models do not allow one to determine the mechanisms regulating spontaneously arising PNAd$^+$ vasculature. In non-transgenic tumor models, the density of intratumoral DCs[22] and Treg depletion[23] have been associated with the presence of LN-like vasculature, but the mechanisms controlling its development remain unknown.

Although it is generally assumed that tumor-infiltrating CD8 T-cells are effector cells that differentiated in tumor-draining LN, we previously showed that naïve T-cells also infiltrate tumors[24]. Tumor infiltrating naïve T-cells differentiate into functional effector cells in the tumor[24] and promote its destruction[25,26]. However, this work did not establish the mechanisms that supported naïve T-cell entry. Here we investigated this using murine tumor models established in the absence of transgenic expression of chemokines or cytokines. We show that tumors spontaneously develop LN-like vasculature and identify novel molecular mechanisms, dependent on endogenous effector lymphocytes that drive its formation. We also demonstrate that LN-like vasculature is the major portal through which naïve T-cells enter tumors, and that infiltrating naïve T-cells are able to delay tumor outgrowth. These findings place intratumoral LN-like vasculature in a positive feedback loop that is both a consequence of and contributor to anti-tumor immunity.

RESULTS

Tumors develop LN-like vasculature expressing PNAd and CCL21

Recent studies have identified LN-like vasculature in human tumors as a prognostic marker of enhanced patient survival[3–6]. Thus, we evaluated whether similar vessels developed in murine tumors. By immunofluorescence, we detected PNAd on CD31$^+$ endothelium in subcutaneous (s.c.) and intraperitoneal (i.p.) B16-OVA tumors in C57BL/6 mice (Fig. 1a–c; low-power images in Supplementary Fig. 1a,b). No staining was observed with isotype control antibody (Fig. 1c). PNAd was also expressed on vasculature of LLC-OVA tumors and B16 expressing a tyrosinase epitope as a model antigen (B16-AAD), in both s.c. and i.p. locations (Fig. 1d–g). The fraction of PNAd$^+$ vessels in tumors (~5–10%) was much smaller than in LN (Fig. 1h). PNAd detection on tumor vasculature also required tyramide

amplification, while detection on LN HEV did not, indicating a significantly lower level of expression. In i.p. tumors, a fraction of $PNAd^+$ endothelial cells exhibited the cuboidal morphology typical of LN HEV, with PNAd apparent at both the luminal and abluminal surfaces (Fig. 1i,j). Otherwise, PNAd was expressed on endothelial cells with a flat morphology, typical of the overall tumor vasculature (Fig. 1a,b). To verify that PNAd was expressed on the luminal surface, we injected MECA-79 antibody intravenously before tumor harvest. This labeled the majority of LN HEVs and tumor vessels that in serial sections were $PNAd^+$ based on our standard staining protocol (Fig. 1k,l). No luminal staining was detected after injecting an isotype control antibody (unpublished). In both tumor sites, $PNAd^+$ vessels coexpressed MAdCAM-1 and VCAM-1 (Supplementary Fig. 1c–g). However, VCAM-1 was expressed more highly on PNAd-negative vessels. In i.p. but not s.c. tumors, there were also many vessels that expressed MAdCAM-1 without PNAd (Supplementary Fig. 1e–g). $PNAd^+$ vasculature was also present in genetically induced melanomas from $BRAF^{V600E}$ $PTEN^{-/-}$ transgenic mice[27] (Supplementary Fig. 2a).

We also detected mRNA for chemokines *Ccl21* and *Ccl19* in s.c. and i.p. tumor lysates, although at lower levels than in LN (Fig. 1m). B16-OVA cells cultured *in vitro* did not express detectable levels of either chemokine. CCL21 protein was displayed on the vasculature of all tumors evaluated (Fig. 1n–p), but CCL19 protein was undetectable, likely reflecting the ~10 fold lower expression levels (Fig. 1m). Staining serial sections established that CCL21 was coexpressed on $PNAd^+$ vessels (Fig. 1q). Thus, multiple murine tumor models spontaneously develop LN-like vasculature expressing PNAd and CCL21.

LN-like vasculature enables naïve T-cell infiltration

We previously showed that naïve T-cells directly infiltrated tumors[24], so we tested whether LN-like vasculature served as their entry point. We transferred naïve Thy1.1 congenic OT-I cells into C57BL/6 mice with established s.c. or i.p. B16-OVA tumors, and evaluated the absolute number of infiltrating OT-I cells after 1 hr or 18 hrs. This number was consistent across experiments and largely independent of tumor size (unpublished observations). We used 18 h as a standard time point for most of our experiments, in keeping with other studies[28–31]. However, infiltration was largely complete by 1 h (Fig. 2a). Co-transferred naïve ($CD44^{lo}$) polyclonal T-cells infiltrated tumors equivalently to naive OT-I cells, demonstrating that infiltration was not dependent on antigen specificity (Fig. 2b). The efficiency of naïve T-cell infiltration into tumors was lower than into LN, however, consistent with the lower PNAd expression on tumor vasculature (Fig. 2c).

Disruption of chemokine signaling in transferred naïve OT-I cells by pertussis toxin pretreatment prevented their infiltration into tumors (Fig. 2d), indicating entry is chemokine dependent. To directly determine if naïve T-cell infiltration required interactions with LN-like vasculature, OT-I cells were pretreated with either anti-L-selectin or anti-CCR7 blocking antibodies prior to adoptive transfer. T-cell entry into LN and both s.c. and i.p. tumors was significantly inhibited when either molecule was blocked (Fig. 2e–g). CCR7 signaling activates integrin LFA-1 to cause arrest and extravasation via interactions with ICAM-1[32]. ICAM-1 was widely expressed on tumor vessels (unpublished observations), and pretreatment of naïve OT-I cells with anti-CD11a to block LFA-1 also prevented infiltration

into both LN and tumors (Fig. 2e–g). To determine if infiltration was mediated by L-selectin binding to MAdCAM-1 or PNAd, we transferred OT-I cells into i.p. tumor bearing mice pretreated to block luminally expressed molecules with injection of either anti-MAdCAM-1, anti-PNAd or isotype control. MAdCAM-1 blockade reduced infiltration into Peyer's Patches but had no effect on tumor infiltration (Fig. 2h). In contrast, blockade of luminal PNAd abolished naïve T-cell infiltration into both inguinal LN and tumors (Fig. 2i). These results demonstrate that naïve T cells infiltrate tumors by adhering to $PNAd^+$ vasculature.

PNAd and CCL21 in tumors do not require LTβR signaling

Luminal PNAd expression on LN HEVs is primarily controlled by LTβR signaling[8]. To determine if this pathway controlled PNAd in tumors, we blocked it throughout i.p. tumor outgrowth using a LTβR-Ig fusion protein[25]. This did not affect overall LN vascularity (Fig. 3a,b), but significantly decreased PNAd expression on LN vessels and resulted in loss of HEV morphology (Fig. 3a,c). As expected, residual PNAd on flat endothelium in LTβR-blocked mice was abluminal, while PNAd on control HEV was displayed on both luminal and abluminal surfaces (Fig. 3a). In a parallel group of LTβR-Ig treated mice that received naïve OT-I T-cells, loss of luminal PNAd led to significantly reduced LN infiltration (Fig. 3d). However, LTβR-Ig blockade had no effect on PNAd expression on i.p. tumor vasculature (Fig. 3e–g). Concordantly, naïve OT-I cells transferred to a parallel cohort of LTβR-blocked animals entered i.p. tumors in greater numbers than controls, demonstrating that PNAd was still expressed on the luminal surface (Fig. 3h). LTβR-Ig treatment did not alter expression of *Ccl21* in either LN or tumors (Fig. 3i,j). Thus, the mechanisms that control luminal PNAd on LN HEV and tumor vasculature are distinct.

CD8 T-cells induce LN-like vasculature in i.p. tumors

To elucidate mechanisms underlying the development of LN-like vasculature in tumors, we investigated whether immune cell subsets were involved. Infiltration of transferred naïve OT-I and naïve polyclonal T-cells into i.p. tumors growing in $Rag2^{-/-}$ mice, which lack endogenous B and T lymphocytes, was significantly decreased (Fig. 4a,b). However, naïve T-cells infiltrated i.p. tumors grown in B-cell deficient $\mu MT^{-/-}$ mice normally (Fig. 4c). Furthermore, infiltration into i.p. tumors in $\beta 2M^{-/-}$ mice, which retain B-cells and CD4 T-cells but lack endogenous CD8 T-cells and NKT-cells, was poor (Fig. 4b). However, infiltration into i.p. tumors in $CD1d^{-/-}$ mice was normal, ruling out a requirement for NKT-cells and pinpointing CD8 T-cells as necessary (Fig. 4d). A role for CD8 T-cells in induction of LN-like vasculature was also suggested in genetically induced melanomas from $BRAF^{V600E}$ $PTEN^{-/-}$ transgenic mice. These tumors are well infiltrated by endogenous CD8 T-cells[33], and the majority contained $PNAd^+$ vasculature (Supplementary Fig. 2b). In contrast, tumors from $BRAF^{V600E}$ $PTEN^{-/-}$ mice with an activating mutation in β-catenin[34] are devoid of infiltrating CD8 T-cells[35], and none of these tumors contained $PNAd^+$ vasculature (Supplementary Fig. 2b).

To directly establish the importance of endogenous CD8 T-cells, we reconstituted $Rag2^{-/-}$ mice with total CD8 T-cells purified from C57BL/6 mice prior to implantation of i.p. tumors. We then assessed development of LN-like vasculature directly by measuring expression of PNAd and CCL21 and indirectly by monitoring infiltration of transferred

naïve OT-I cells, in separate cohorts of mice (Fig. 4e). PNAd was completely absent from i.p. tumor vasculature in *Rag2*$^{-/-}$ mice, and expression of *Ccl21* was significantly decreased (Fig. 4f–h). In i.p. tumors from CD8-repleted *Rag2*$^{-/-}$ mice, however, expression of PNAd and *Ccl21* and infiltration of transferred naive OT-I cells were restored to levels seen in wild type mice (Fig. 4f–i). It seemed likely that this was directly mediated by CD8 effector T-cells from the repleting pool that had infiltrated the tumor, because equivalent numbers of endogenous CD8 T-cells were found in tumors in repleted *Rag2*$^{-/-}$ mice and C57BL/6 mice (Fig. 4j). In keeping with this, B16-F1 tumors, which lack a strong antigen, show reduced infiltration by endogenous CD8 T-cells in C57BL/6 mice, compared to B16-OVA tumors (Fig. 4k,l). In addition, PNAd expression on B16-F1 tumor vasculature was significantly lower than on B16-OVA vasculature, but still greater than in B16-OVA tumors from Rag2$^{-/-}$ mice (Fig. 4m). These data establish that PNAd and CCL21 expression on i.p. tumor vasculature is determined by the extent of infiltration of endogenous effector CD8 T-cells, which is in turn related to the strength of the antigenic stimulus that activates them.

CD8 T and NK cells induce LN-like vasculature in s.c. tumors

In contrast to i.p. tumors, transferred naïve OT-I cells infiltrated s.c. tumors in control and *Rag2*$^{-/-}$ mice equivalently, while s.c. tumors in *β2M*$^{-/-}$ hosts continued to be poorly infiltrated (Fig. 5a). This suggested that NK cells, which are hyporesponsive in *β2M*$^{-/-}$ but not *Rag2*$^{-/-}$ animals[36,37], acted redundantly with endogenous CD8 T-cells to induce LN-like vasculature in s.c. tumors. Indeed, while depletion of NK cells from wild type mice had no effect, naïve T-cell infiltration into s.c. tumors was significantly diminished when NK cells were depleted from *Rag2*$^{-/-}$ mice, and restored in NK-depleted *Rag2*$^{-/-}$ mice reconstituted with CD8 T-cells (Fig. 5b,c). In addition, PNAd and *Ccl21* expression was significantly decreased in s.c. tumors from NK-depleted *Rag2*$^{-/-}$ mice (Fig. 5d–f). Therefore, NK cells act redundantly with endogenous CD8 T-cells to induce LN-like vasculature in s.c. tumors.

Cytokine production differs between tumor sites

Equivalent numbers of NK cells and CD8 T-cells were present in both i.p. and s.c. tumors, demonstrating that NK induction of LN-like vasculature in s.c. but not i.p. tumors was not due to differential representation (Fig. 5g). To assess the effector activities of these cells, we treated tumor-bearing mice with Brefeldin A for 4 h and analyzed the *in vivo* cytokine profiles immediately after harvest. About 20% of CD8 T-cells in both tumor locations produced IFNγ (Fig. 5h). However, while ~30% of NK cells in s.c. tumors produced IFNγ, less than 5% of NK cells in i.p. tumors did so (Fig. 5h). In addition, significantly larger fractions of NK cells and CD8 T-cells produced TNFα in s.c. tumors than in i.p. tumors (Fig. 5i). Thus, NK and effector CD8 T-cell functional activities depend on the location of tumor growth, and the involvement of NK cells in inducing LN-like vasculature correlates with their secretion of IFNγ.

IFNγ controls CCL21 but not PNAd expression in i.p. tumors

We therefore tested whether effector lymphocyte-derived IFNγ induced LN-like vasculature. Naïve OT-I cells failed to infiltrate i.p. tumors in *IFNγ*$^{-/-}$ hosts or in WT mice treated with

IFNγ-neutralizing antibody (Fig. 6a,b). However, infiltration into s.c. tumors in *IFNγ*$^{-/-}$ mice was unimpaired (Fig. 6c). Reconstitution of *Rag2*$^{-/-}$ mice with *IFNγ*$^{-/-}$ CD8 T-cells prior to tumor implantation failed to rescue infiltration of adoptively transferred naïve OT-I into established i.p. tumors (Fig. 6d), even though the repleted *IFNγ*$^{-/-}$ CD8 T-cells were present in tumors in normal numbers (Fig. 6e). Surprisingly, PNAd was still expressed on tumor vasculature in these mice (Fig. 6f,g). In contrast, *Ccl21* expression was significantly reduced (Fig. 6h,j). *Ccl19* expression was not significantly different in i.p. tumors from WT and *IFNγ*$^{-/-}$ mice (Fig. 6i), demonstrating that its low level expression (Fig. 1m) was insufficient to mediate naïve T-cell recruitment. Thus, IFNγ secretion by endogenous CD8 T effectors controls only one element of LN-like vasculature in i.p. tumors.

IFNγ controls CCL21 expression by CD31$^+$ and gp38$^+$ cells

In LN, CCL21 is produced by gp38$^+$CD31^{neg} fibroblastic reticular cells (FRC), gp38$^+$CD31$^+$ lymphatic endothelial cells (LEC) and gp38^{neg}CD31$^+$ HEV[1]. Both i.p. and s.c. tumors contained gp38$^+$CD31^{neg} cells (Fig. 7a), which also expressed other markers of LN FRC and fibroblasts, including CD140a, CD44, and VCAM-1[38] (Fig. 7b). Tumors also contained CD31$^+$ blood endothelial cells but very few gp38$^+$CD31$^+$ LEC (Fig. 7a). *Ccl21* was expressed by sorted gp38$^+$ fibroblasts and CD31$^+$ endothelial cells (Fig. 7c). All other examined cells, including CD45^{neg}gp38^{neg}CD31^{neg} cells (which includes tumor cells), CD11c$^+$ dendritic cells, and other CD45$^+$ cells, expressed little to no *Ccl21* (Fig. 7c). Based on cell numbers and per cell expression, gp38$^+$ cells were the major source of CCL21 in both i.p. and s.c. tumors. Both gp38$^+$ and CD31$^+$ cells also expressed IFNγR1 (Fig. 7d), suggesting they could respond directly to IFNγ. Indeed, *Ccl21* expression by both of these radioresistant cells was significantly decreased in i.p. tumors from WT➔*IFNγR1*$^{-/-}$ bone marrow chimeras, compared to reciprocal chimeras in which only hematopoietic cells lacked IFNγR1 (Fig. 7e). These data support a model in which IFNγ secreted by CD8 effectors in i.p. tumors directly induces CCL21 in both gp38$^+$ fibroblasts and endothelial cells.

LTα$_3$-TNFR signaling induces PNAd on tumor vasculature

It remained unclear how effector lymphocytes induced PNAd expression on tumor vasculature independently of LTβR and IFNγ. Although TNFα was also secreted by endogenous effector lymphocytes (Fig. 5), PNAd expression and naïve T-cell infiltration were normal in i.p and s.c. tumors grown in TNFα$^{-/-}$ hosts (Fig. 8a–c). In contrast, PNAd expression and naïve T-cell infiltration were significantly decreased in tumors growing in TNF receptor 1/2 (*TNFR1/2*$^{-/-}$) dual knockout hosts (Fig. 8a–d). *Ccl21* levels were also significantly reduced (Fig. 8e). This suggested that homotrimeric LTα$_3$, the other known ligand for TNFR1 and TNFR2, was responsible for inducing PNAd on tumor vasculature. Effector CD8 T-cells sorted from i.p. and s.c. tumors expressed *Lta* mRNA at higher levels than *Tnfa* (Fig. 8f). We repleted *Rag1*$^{-/-}$ mice with *TNFα*$^{-/-}$ or *LTα*$^{-/-}$ CD8 T-cells and evaluated PNAd expression on subsequently implanted i.p. tumor vasculature. Representation of all repleted endogenous CD8 T-cells in tumors was comparable to that of controls (Fig. 8g). *TNFα*$^{-/-}$ CD8 T-cells restored PNAd to levels seen in tumors from wild type mice (Fig. 8h). *LTα*$^{-/-}$ CD8 T-cells, however, failed to significantly induce PNAd expression (Fig. 8h). Intratumoral CD31$^+$ endothelial cells expressed TNFR1 but little TNFR2 (Fig. 8i). Using WT➔*TNFR1/2*$^{-/-}$ and reciprocal bone marrow chimeras, PNAd

expression on i.p. tumor vasculature was deficient only when endothelial cells did not express TNFRs (Fig. 8j). These results suggest a model in which $LT\alpha_3$ released by effector lymphocytes directly engages TNFR1 on tumor endothelium to induce PNAd expression.

Tumor infiltrating naïve T-cells delay tumor outgrowth

We next determined whether naïve T-cells that infiltrated tumors via LN-like vasculature exerted a positive or negative effect after differentiating in the tumor mass. We transferred naïve OT-I cells into C57BL/6 or *TNFR1/2*$^{-/-}$ mice bearing early (d 8) s.c. B16-OVA tumors and monitored outgrowth and survival. At the time of naïve T-cell transfer, we also initiated daily treatment with the sphingosine 1-phosphate receptor modulator FTY720, which efficiently prevents the egress of naïve and activated lymphocytes from secondary lymphoid organs[39–42]. This setup allowed early infiltration of endogenous effectors necessary to induce LN-like vasculature, but prevented their ongoing egress from tumor draining LN into the tumor mass after the time of naïve T-cell transfer. It also prevented the tumor infiltration of OT-I T-cells that became activated in tumor draining LN. Thus, it allowed us to assess the activity of naïve OT-I T-cells that directly infiltrated the tumor via LN-like vasculature. The efficacy of FTY720 treatment was confirmed by examining the percentage of OT-I cells expressing high levels of CD44, a marker of antigen experience, in different LN beds. This percentage was high and similar in the tumor draining inguinal LN of vehicle treated and FTY720-treated mice (Fig. 9a). However, CD44-expressing OT-I cells in the antigen free mesenteric LN, which redistribute from the tumor-draining LN[42], were reduced by over 80% by FTY720 treatment (Fig. 9a). Despite sequestration of LN-activated effector T-cells, naïve OT-I cells that entered tumors in wild type mice via LN-like vasculature significantly delayed tumor outgrowth and prolonged survival (Fig. 9b,c). In contrast, naïve OT-I cells had no effect on tumors in *TNFR1/2*$^{-/-}$ hosts, which lack LN-like vasculature (Fig. 9b,d). Thus, naïve CD8 T-cells that infiltrate tumors via LN-like vasculature enhance anti-tumor immunity. This is consistent with our previous demonstration that they become fully differentiated intratumoral effector cells[24].

Organized lymphoid tissue develops in i.p. tumors

Because PNAd and CCL21 expression in inflamed tissues has been associated with formation of TLO, we determined whether this also occurred in tumors. In i.p. tumors, we found large follicular aggregates of B lymphocytes immediately surrounding some, but not all sites of PNAd expression (Fig. 10a). These aggregates were co-extensive with a reticular network of gp38^{+} cells that did not stain for the LEC marker LYVE-1 (Fig. 10a), suggesting that they represented the gp38^{+}CD31^{neg} CCL21^{+} FRC-like cells identified by flow cytometry (Fig. 7a). T-cells and DC were also found in these structures, but they were not organized into a discreet zone (Fig. 10b,c), as has been seen in some TLO. Nonetheless, in conjunction with our earlier work[24], these results suggest that organized lymphoid tissue associated with LN-like vasculature may serve as sites for the activation and regulation of recently entering naïve T-cells.

DISCUSSION

Our observation of LN-like vasculature in multiple tumor models adds to a growing body of literature demonstrating its presence in mouse[21,23] and human[4,6,43] tumors. The presence of PNAd and CCL21 positive LN-like vasculature in human tumors has been associated with a positive prognosis. We also previously showed that naïve T-cells enter tumors and differentiate into effectors[24]. Here we link these two observations, demonstrating that PNAd and CCL21 control naïve T-cell entry into tumors. In contrast to LN HEV and many TLO models, development of intratumoral LN-like vasculature did not depend upon LTβR signaling. Instead, it depended on other cytokines secreted by tumor infiltrating CD8 or NK effector lymphocytes. PNAd on tumor endothelium was induced by $LT\alpha_3$ signaling through TNFRs. CCL21 expression by endothelial cells and associated $gp38^+$ fibroblasts was induced by IFNγ downstream of TNFR signaling in i.p. tumors. However, its control in s.c tumors is more complex. It likely involves IFNγ, which is made by both CD8 T-cells and NK cells in these tumors, and redundant factor(s) that remain to be identified. Interestingly, effector functions of intratumoral NK cells also varied with location of tumor growth, altering their ability to induce PNAd and CCL21 expression. Our results support a model in which an initial influx of lymph-node primed effector lymphocytes into the tumor induces the development of LN-like vasculature, which supports recruitment of naïve T-cells that contribute to ongoing anti-tumor immunity.

Control of PNAd expression on LN HEV and in TLO models has been primarily attributed to DCs that express $LT\alpha_1\beta_2$, which engages LTβR[7,8,13,14]. PNAd expression in human breast cancer has also been correlated with the presence of LTβ-producing DCs[22]. Other reports have also demonstrated a role for B cells in inflamed LN[44,45], and an indirect role for CD4 T-cells by initiating DC-mediated induction of PNAd in a thyroiditis TLO model[18]. However, our results with mice deficient in effector lymphocyte populations clearly demonstrate that the simple presence of DCs is insufficient for inducing PNAd expression in B16 tumors. Similarly, neither B cells nor CD4 T cells are necessary or sufficient for inducing PNAd in this tumor model system. Instead, PNAd expression required endogenous effector CD8 T-cells in i.p. tumors, and either CD8 T-cells or NK cells in s.c. tumors. Effector lymphocytes acted directly to induce PNAd by secreting $LT\alpha_3$, which engaged TNFRs on endothelial cells. The expression of TNFR1 rather than TNFR2 on endothelial cells in B16 tumors suggests that signaling through this receptor is responsible.

Another recent report showed PNAd expression in MCA-induced tumors required Treg depletion, although the molecular mechanism controlling PNAd expression was not defined[23]. In B16 tumors growing in wild type mice, and in genetically induced melanomas, however, PNAd is expressed despite the presence of Treg cells. Taken together, we suggest that the role of Tregs in regulating PNAd is indirect, by limiting the accumulation and/or effector activities, including $LT\alpha_3$ secretion, of activated lymphocytes. That Treg depletion was not required for PNAd expression in these melanoma models likely reflects in part the differences in antigenic strength between ovalbumin and neoantigens formed in genetically induced melanomas or MCA-induced fibrosarcomas, tipping the balance towards more robust effector activity. Consistent with this, weakly antigenic B16-F1 tumors had reduced

accumulation of effector lymphocytes and lower levels of PNAd expression than B16-OVA tumors.

At the molecular level, LTβR signaling is critical for regulating PNAd expression on LN HEV[8] and in several TLO models[9–12,46]. Previous work by Ruddle and colleagues also dissected the roles of LTα and LTβ using a model of transgenic overexpression in the pancreas and kidney[15,16,47,48]. In those studies, a primary role for LTβR signaling was also demonstrated, as PNAd$^+$ vasculature was not seen when the LTα-transgene was expressed in the absence of LTβ[15]. Abluminal PNAd was present when only the LTα-transgene was expressed in mice with endogenous LTβ, while luminal PNAd was dependent on transgenic expression of both LTα and LTβ[16]. In other circumstances, however, PNAd expression can be LTβR-independent. For example, when LTβR is deleted from endothelial cells, PNAd remains present on cells that have otherwise lost the typical HEV morphology[49]. PNAd is also expressed on the abluminal surface of LN HEV in LTβ knockout animals[16] or mice treated with LTβR-Ig[8,45]. A role for $LT\alpha_3$-TNFR signaling in controlling this residual abluminal PNAd has been suggested[16] but not directly demonstrated. Here, we have shown that PNAd expression on tumor-associated LN-like vasculature is LTβR-independent and $LT\alpha_3$-TNFR-dependent.

Other characteristics of LN-like vasculature in tumors differ from LN HEV or other TLO models. First, PNAd expression levels on tumor vasculature are low compared to LN HEV, and PNAd in tumors was largely expressed on flat endothelium. Importantly, $LT\alpha_3$-induced PNAd on tumor vasculature was clearly luminal, enabling L-selectin mediated naïve T-cell infiltration that could be blocked by i.v administration of PNAd antibody. LN-like vasculature co-expressed MAdCAM-1, which is found on HEV in mesenteric LN and is also induced by $LT\alpha_3$[15,47]. MAdCAM-1 did not contribute to naïve T cell infiltration, however, perhaps because it is not properly post-translationally modified to serve as an L-selectin ligand. A critical step in the generation of PNAd is the sulfation of core glycoproteins by the sulfotransferases GlcNAc6ST-1 and GlcNAc6ST-2[50]. GlcNAc6ST-2 is expressed specifically in HEV and is primarily responsible for generating luminal PNAd[51]. GlcNAc6ST-1 is expressed more widely and contributes to both luminal and abluminal PNAd[52–54]. Our finding of low-level expression of PNAd on both luminal and abluminal surfaces suggest the induction of GlcNAc6ST-1 rather than GlcNAc6ST-2 by $LT\alpha_3$-TNFR signaling. In any case, molecular control of PNAd expression on tumor vasculature appears distinct from what has been reported in other systems, perhaps as a consequence of disregulated angiogenesis.

A second component of lymph node HEV expressed on tumor vasculature was the chemokine CCL21. CCL21 expression has also been reported in human tumors[3,4,6], but like PNAd, its regulation and role in the tumor microenvironment is poorly understood. CCL21 expression depends on TNFα and LT in the spleen[55,56] and transgenic TLO models[16,57], but its expression in adult LN is independent of these cytokines[8,45], and no alternative regulatory mechanisms have been defined. In tumors, CCL21 expression was controlled by effector lymphocytes, and in i.p. tumors, required both TNFR signaling and CD8 effector secretion of IFNγ. We are not aware of other reports that CCL21 is induced by IFNγ. In fact, one report demonstrated that IFNγ was required for a transient drop in CCL21 levels in the

inflamed spleen[58]. Nevertheless, our data suggest that IFNγ directly induces CCL21 expression in both endothelial cells and gp38$^+$ cells associated with LN-like vasculature. Because i.p. tumors in *TNFR1/2*$^{-/-}$ mice lack both PNAd and CCL21 while i.p. tumors in *IFNγ*$^{-/-}$ mice are deficient in CCL21 only, initial LTα$_3$-TNFR signaling may enable subsequent responsiveness of CCL21 expression to IFNγ signaling.

CCL21 expression by gp38$^+$ cells is intriguing, because these cells share phenotypic characteristics with LN FRC[38], which are a major source of CCL21 in LN. gp38$^+$ cells were also the major source of CCL21 in tumors, but were in proximity to PNAd$^+$ endothelial cells that also expressed CCL21 on their own. Thus, CCL21 displayed on LN-like vasculature that enables naïve T-cell entry likely reflects both direct production by the endothelium and CCL21 transcytosed[59] from adjacent gp38$^+$ cells. We also found that these gp38$^+$ cells are organized around portions of LN-like vasculature into reticular networks in conjunction with large aggregates of B lymphocytes in i.p. tumors. The functionality of gp38$^+$ cells as components or organizers of these TLO-like structures, the functionality of the structures themselves, and the reasons they develop at only some sites of LN-like vasculature, remain to be defined. Nonetheless, these observations point towards a level of immune organization within tumors that may offer additional targets for intervention.

The cellular and molecular differences in induction of LN-like vasculature in i.p. and s.c. tumors highlight a microenvironmental heterogeneity that depends on the location of growth. This is typified by the greater secretion of IFNγ and TNFα by NK cells in s.c. tumors, enabling them to induce LN-like vasculature in this location. The enhanced functionality of NK cells in s.c. tumors could reflect the recruitment of distinct NK subpopulations that cannot reach i.p. tumors based on differential expression of chemokine receptors[60]. Alternatively, each location may display different levels of activating or inhibitory NK receptor ligands[61], shifting the balance in s.c. tumors towards NK cell activation. The presence of immunosuppressive cytokines in i.p. tumors such as TGFβ could also inhibit NK cell effector activities. These differences may be driven by properties of the tumor microenvironment that are determined by external cues, as has been described in the regional control of DC programming of tissue selective T cell trafficking[62]. Location-based microenvironmental heterogeneity may affect efforts to enhance immune responses in various metastatic sites.

Evidence for both positive and negative effects of LN-like vasculature on anti-tumor immunity have been reported in murine models[20,21]. In several human studies, PNAd and CCL21 expression have been associated with a positive prognosis[3–6]. Because our results demonstrate that the level of LN-like vasculature is correlated with the extent of accumulation by endogenous effector lymphocytes that induce it, this prognostic association could simply reflect that the presence of LN-like vasculature is a proxy for effector lymphocyte infiltration. Here, however, we have shown that the development of LN-like vasculature directly supports an ongoing anti-tumor response by enabling the infiltration of naïve CD8 T-cells, which can differentiate into effector cells in the tumor microenvironment. It is important to note that our demonstration of this effect occurred in an experimental setup that necessarily eliminated the normal constant traffic of LN-activated effectors, as well as any ongoing traffic of naïve T-cells, into the tumor. The overall impact

of a more sustained influx of naïve tumor infiltrating CD8 T-cells may therefore be even greater. Thus, induction of LN-like vasculature in tumors has the potential to be a key contributor to anti-tumor immunity by generating a self-sustaining infiltration of T-cells into the tumor mass.

METHODS

Mice

Female C57BL/6 mice (NCI); *OT-I Rag1*$^{-/-}$, *Rag2*$^{-/-}$, and *TNFα*$^{-/-}$ mice (Taconic); Thy1.1 congenic, $\beta_2M^{-/-}$, *IFNγ*$^{-/-}$, *Rag1*$^{-/-}$, *μMT*$^{-/-}$, *IFNγR1*$^{-/-}$, *LTα*$^{-/-}$ and *TNFR1/2*$^{-/-}$ mice (Jackson); and *CD1d*$^{-/-}$ mice (gift from Victor Laubach, University of Virginia) were bred and maintained under specific pathogen free conditions. All gene knockout mice were on a C57BL/6 background. Animals were used at approximately 8–12 weeks of age. All protocols were approved by the University of Virginia Institutional Animal Care and Use Committee.

Tumor cells and injections

B16-F1 melanoma cells, variants expressing cytoplasmic ovalbumin (B16-OVA) or a chimeric MHC molecule that presents tyrosinase (B16-AAD), and Lewis lung carcinoma (LLC) cells expressing OVA (a gift from E. Podack, University of Miami) (4×10^5 cells) were injected i.p. or s.c. Tumors were allowed to establish for ~14 days prior to naïve T-cell transfer or other analyses. Paraffin embedded melanomas from $BRAF^{V600E}$ $PTEN^{-/-}$ mice and $BRAF^{V600E}$ $PTEN^{-/-}$ with an activating mutation in β-catenin[27,34] were a kind gift from Dr. Marcus Bosenberg (Yale).

Treatments of tumor bearing mice

Anti-IFNγ[63] (250 μg) was injected i.p. every 7 d beginning 1 d prior to tumor implantation. LTβR-Ig fusion protein[25] (100 μg) was injected i.p. every 4 d, beginning 1 d prior to tumor implantation. NK cells were depleted by injection of 100 μg anti-NK1.1 (PK136, BioXcell) every 3 d beginning 3 d prior to tumor implantation. For repletion of *Rag*$^{-/-}$ mice, CD8 T-cells purified from pooled LN and spleen by magnetic bead enrichment on an autoMACS Cell Separator (Miltenyi Biotec) (5×10^6 cells) were injected i.v. ~3 d prior to tumor implantation.

Adoptive transfer of naïve T-cells

Naïve OT-I T-cells isolated from pooled LN and spleen of *OT-I RAG1*$^{-/-}$*/Thy1.1* mice (4×10^6 cells) or polyclonal $CD8^+$ T-cells pooled from LN and spleen of C57BL/6 mice and depleted of CD44 expressing cells by magnetic beads (Miltenyi) were injected into the lateral tail vein of recipients. In blocking experiments, cells were incubated with 100 ng/mL pertussis toxin (PTX, Sigma) for 1 h at 37°C, or 100 μg of rat IgG (Jackson Immunoresearch), anti-CD62L (Mel-14, ATCC), or anti-CD11a (M17/4, BioXcell), or 50 μg of anti-CCR7 (4B12, eBioscience) and washed before injection. Luminal PNAd or MAdCAM-1 were blocked by injection of 100 μg of anti-MAdCAM-1 (MECA-367, BioXcell), anti-PNAd (MECA-79, BioLegend) or isotype Rat IgG or IgM i.v. 1 h prior to T-

cell transfer. In some experiments, cells were labeled with Cell Trace Violet (CTV) (Invitrogen) prior to transfer. Tissues were harvested 1 h or 18 h after naïve T-cell transfer.

Flow cytometry and cell sorting

LN were homogenized before staining. Tumors were incubated with 0.5 mg/mL Collagenase A (Roche) and 60 U/mL DNase I (Sigma-Aldrich) for 30 minutes at 37°C, homogenized and lymphocytes isolated on Lympholyte-M (Cedarlane). Single cell suspensions were treated with anti-CD16/32 (2.4G2, BioXcell) to block Fc receptors; and then with one or more of the following fluorescently conjugated antibodies (0.25 – 2 μg mL^{-1}): CD8α (53-6.7), Thy1.1 (HIS51), CD69 (H1.2F3), CD25 (PC61.5), CD44 (IM7), IFN-γ (XMG1.2), TNFα (MP6-XT22), CD3ε (145-2C11), CD45 (30-F11), CD45.1 (A20), CD45.2 (104), CD11c (N418), CD11b (M1/70), TNFR2 (TR75-54), gp38 (8.1.1), CD31 (390), IFNγR1 (2E2), CD140a (APA5), VCAM-1 (429), NK1.1 (PK136), CD49b (DX5), Ter119 (all from eBioscience), CD4 (GK1.5) (BD Biosciences), Thy1.2 (30-H12) and TNFR1 (55R-286) (BioLegend). Live/Dead Aqua (Invitrogen) or DAPI (Sigma) were used to exclude dead cells from analysis. Samples were run on a FACSCanto II (BD) and analyzed using FlowJo software (TreeStar). For sorting experiments, single cell suspensions of tumors were pre-enriched using magnetic beads and then sorted to high purity on an Influx cell sorter (BD) directly into RNAProtect (Qiagen). Blood endothelial cells were gated as live singlet $Ter119^{-}CD45^{-}gp38^{-}CD31^{+}$. $Gp38^{+}$ cells were gated as live singlet $Ter119^{-}CD45^{-}gp38^{+}CD31^{-}$.

In vivo effector function

Tumor bearing mice were injected i.p. with 250 μg of Brefeldin-A (Sigma-Aldrich). 4 h later, tumor-infiltrating lymphocytes were isolated as described above and stained for surface molecule expression, then stained for intracellular IFN-γ or TNF-α using CytoFix/CytoPerm (BD Biosciences).

Immunofluorescence Microscopy

Tissues were flash frozen in liquid nitrogen, embedded in OCT and cut into 6 μm sections. Sections were fixed with acetone/ethanol and blocked with PBS/5% BSA, anti-CD16/32, 3% H_2O_2, 0.1% NaN_3, and Avidin/Biotin Blocking Kit (Vector Laboratories). Paraffin embedded melanomas from $BRAF^{V600E}$ $PTEN^{-/-}$ mice were deparaffinized, rehydrated, and subjected to heat-induced antigen retrieval for 20 minutes at 95°C in citrate buffer, pH 6.0 before blocking steps. Sections were stained with biotinylated or fluorescence conjugated antibodies (5 – 20 μg mL^{-1}) to CD31 (390), ICAM-1 (YN1/1.7.4), CD11c (N418), CD3ε (145-2C11), CD8α (53-6.7), B220 (RA3-6B2), LYVE-1 (ALY7), gp38 (8.1.1), MAdCAM-1 (MECA-367), VCAM-1 (429) (eBioscience), PNAd (MECA-79) (BioLegend), CCL21 (R&D Systems) antibodies or appropriate isotype control antibodies followed by peroxidase or fluorescent Streptavidin conjugates (Jackson Immunoresearch). PNAd and CCL21 signals in frozen tumor sections were amplified with Tyramide Signal Amplification Plus kits (PerkinElmer). PNAd signals in paraffin embedded sections were detected using DAB/Ni substrate (Vector) and slides were counterstained in Hematoxylin QS (Vector). For luminal PNAd staining, 100 μg of MECA-79 or Rat IgM was injected i.v. 30 minutes prior to tumor harvest. Slides were mounted in SlowFade Gold (Invitrogen) and

images collected on a Microphot-FXA (Nikon) with Qcolor 5 CCD camera (Olympus) or AxioImager with Apotome (Zeiss).

Image Analysis

Quantification of $CD31^+$ and $PNAd^+$ areas was performed using ImageJ software (NIH) on original fluorescence images taken at identical exposures across samples. Consistent thresholds were applied to each image to identify $CD31^+$ and $PNAd^+$ pixels. The percentage of $CD31^+$ pixels of total imaged area, and the percentage of $PNAd^+$ pixels within the region of interest of $CD31^+$ area was calculated. Quantification of CD8 T-cell infiltration was performed by counting the number of cells present per 20X field. Multiple sections per tumor and random fields per section were used for analysis. For image presentation, brightness and contrast were linearly adjusted and color-merged images were generated using Photoshop CS6 software (Adobe).

RT-PCR

RNA and a blend of oligo (dT) and random hexamer primers were used to generate cDNA (iScript cDNA Synthesis Kit, BioRad). Amplification was performed using iQ SYBR Green Supermix (BioRad) on a MyiQ qPCR Detection System (BioRad) with the following program: 95°C for 10 min; 40 cycles of 95°C for 30 s, 60°C for 1 min. Primers used were the following: *Hprt* forward, 5'- AGGTTGCAAGCTTGCTGGT-3', and reverse, 5'-TGAAGTACTCATTATAGTCAAGGGCA-3'; *Ccl21* forward, 5'-CAAGGGCTGCAAGAGAACTG-3', and reverse, 5'-TGTGAGTTGGACCGTGAACC-3'; *Ccl19* forward, 5'-GCCTCAGATTATCTGCCAT-3', and reverse, 5'- ATCATTAGCACCCCCCAGAG-3'; *Lta* forward, 5'-AAACCTGCTGCTCACCTTGT-3' and reverse, 5'-AGAGAAGCCATGTCGGAGAA-3'; *Tnfa* forward, 5'- CCAAAGGGATGAGAAGTTCC-3' and reverse, 5'-CACTTGGTGGTTTGCTACGA-3'. Data is presented as $2^{\wedge-\Delta\Delta C_t}$ or $2^{\wedge-\Delta\Delta C_t}$ relative to *Hprt* as described in legends.

Bone marrow chimeras

Mice were irradiated (650 rad x 2) and reconstituted with a minimum of 2×10^6 bone marrow cells depleted of $CD4^+$ and $CD8^+$ T-cells by magnetic beads (Miltenyi Biotec). Chimeras were maintained on Sulfatrim (sulfamethoxazole/trimethoprim) water for 3 weeks, and allowed to reconstitute for at least 8 weeks prior to use.

Tumor control

B16-OVA tumors were implanted s.c. into WT or *TNFR1/2*$^{-/-}$ mice. On d 8 after implantation, mice were injected i.v. with 4×10^6 OT-I/Thy1.1 cells depleted of CD44 expressing cells by magnetic beads and treated daily with 1 mg kg^{-1} FTY720 (a gift from V. Brinkmann, Novartis Pharma AG, Basel, Switzerland) in sterile saline i.p., or treated with FTY720 without receiving naïve T-cells. Tumor size was monitored daily by caliper measurements, and mice were sacrificed when tumors reached 16 mm in any one dimension.

Statistical Analysis

P values were calculated for comparisons between two groups by unpaired *t*-tests, and for comparisons between three or more groups by one-way analysis of variance (ANOVA) with post tests to correct for multiple comparisons as indicated in legends. $p<0.05$ was considered statistically significant. All graphs and statistics were calculated using Graph Pad Prism version 6.0.

Supplementary Material

Refer to Web version on PubMed Central for supplementary material.

ACKNOWLEDGEMENTS

We thank Holly Davis for animal husbandry, Dr. Kara Cummings for laboratory support, and the entire Engelhard laboratory for insightful discussions and advice. We thank Dr. Kodi Ravichandran for advice in preparing the manuscript and he, along with Dr. Kenneth Tung and Dr. Loren Erickson for use of equipment, the UVA Research Histology Core for tissue sectioning, Dr. E. Podack (University of Miami) for LLC-OVA, Dr. Robert Schreiber (Washington University St. Louis) for IFNγ neutralizing antibody, and Dr. Marcus Bosenberg (Yale) for paraffin-embedded tumors from $BRAF^{V600E}$ $PTEN^{-/-}$ mice and $BRAF^{V600E}$ $PTEN^{-/-}$ with an activating mutation in β-catenin[27,34].

Work was supported by United States Public Health Service (USPHS) grants CA78400 (V.H.E.), training grants GM007267 and AI7496 (E.D.T.), and GM007267, CA009109, and the Farrow Fellowship (J.D.P.).

REFERENCES

1. Girard J-P, Moussion C, Förster R. HEVs, lymphatics and homeostatic immune cell trafficking in lymph nodes. Nat. Rev. Immunol. 2012; 12:762–773. [PubMed: 23018291]
2. Aloisi F, Pujol-Borrell R. Lymphoid neogenesis in chronic inflammatory diseases. Nat. Rev. Immunol. 2006; 6:205–217. [PubMed: 16498451]
3. Coppola D, et al. Unique ectopic lymph node-like structures present in human primary colorectal carcinoma are identified by immune gene array profiling. Am. J. Pathol. 2011; 179:37–45. [PubMed: 21703392]
4. Martinet L, et al. Human solid tumors contain high endothelial venules: association with T- and B-lymphocyte infiltration and favorable prognosis in breast cancer. Cancer Res. 2011; 71:5678–5687. [PubMed: 21846823]
5. Martinet L, et al. High endothelial venules (HEVs) in human melanoma lesions: Major gateways for tumor-infiltrating lymphocytes. Oncoimmunology. 2012; 1:829–839. [PubMed: 23162750]
6. Messina JL, et al. 12-Chemokine gene signature identifies lymph node-like structures in melanoma: potential for patient selection for immunotherapy? Sci. Rep. 2012; 2:765. [PubMed: 23097687]
7. Moussion C, Girard J-P. Dendritic cells control lymphocyte entry to lymph nodes through high endothelial venules. Nature. 2011; 479:542–546. [PubMed: 22080953]
8. Browning JL, et al. Lymphotoxin-beta receptor signaling is required for the homeostatic control of HEV differentiation and function. Immunity. 2005; 23:539–550. [PubMed: 16286021]
9. Gatumu MK, et al. Blockade of lymphotoxin-beta receptor signaling reduces aspects of Sjögren syndrome in salivary glands of non-obese diabetic mice. Arthritis Res. Ther. 2009; 11:R24. [PubMed: 19222863]
10. Gräbner R, et al. Lymphotoxin β receptor signaling promotes tertiary lymphoid organogenesis in the aorta adventitia of aged ApoE−/− mice. J. Exp. Med. 2009; 206:233–248. [PubMed: 19139167]
11. Motallebzadeh R, et al. Blocking lymphotoxin signaling abrogates the development of ectopic lymphoid tissue within cardiac allografts and inhibits effector antibody responses. FASEB J. 2012; 26:51–62. [PubMed: 21926237]

12. Rangel-Moreno J, et al. The development of inducible bronchus-associated lymphoid tissue depends on IL-17. Nat. Immunol. 2011; 12:639–646. [PubMed: 21666689]
13. GeurtsvanKessel CH, et al. Dendritic cells are crucial for maintenance of tertiary lymphoid structures in the lung of influenza virus-infected mice. J. Exp. Med. 2009; 206:2339–49. [PubMed: 19808255]
14. Halle S, et al. Induced bronchus-associated lymphoid tissue serves as a general priming site for T cells and is maintained by dendritic cells. J. Exp. Med. 2009; 206:2593–601. [PubMed: 19917776]
15. Cuff CA, Sacca R, Ruddle NH. Differential induction of adhesion molecule and chemokine expression by LTα3 and LTαβ in inflammation elucidates potential mechanisms of mesenteric and peripheral lymph node development. J. Immunol. 1999; 162:5965–5972. [PubMed: 10229834]
16. Drayton DL, Ying X, Lee J, Lesslauer W, Ruddle NH. Ectopic LTαβ directs lymphoid organ neogenesis with concomitant expression of peripheral node addressin and a HEV-restricted sulfotransferase. J. Exp. Med. 2003; 197:1153–1163. [PubMed: 12732657]
17. Luther SA, et al. Differing activities of homeostatic chemokines CCL19, CCL21, and CXCL12 in lymphocyte and dendritic cell recruitment and lymphoid neogenesis. J. Immunol. 2002; 169:424–433. [PubMed: 12077273]
18. Marinkovic T, et al. Interaction of mature CD3+ CD4+ T cells with dendritic cells triggers the development of tertiary lymphoid structures in the thyroid. J. Clin. Invest. 2006; 116:2622–2632. [PubMed: 16998590]
19. Kim H-J, et al. Establishment of early lymphoid organ infrastructure in transplanted tumors mediated by local production of Lymphotoxin α and in the combined absence of functional B and T cells. J. Immunol. 2004; 172:4037–4047. [PubMed: 15034015]
20. Schrama D, et al. Targeting of Lymphotoxin-α to the tumor elicits an efficient immune response associated with induction of peripheral lymphoid-like tissue. Immunity. 2001; 14:111–121. [PubMed: 11239444]
21. Shields JD, Kourtis IC, Tomei AA, Roberts JM, Swartz MA. Induction of lymphoidlike stroma and immune escape by tumors that express the chemokine CCL21. Science. 2010; 328:749–752. [PubMed: 20339029]
22. Martinet L, et al. High endothelial venule blood vessels for tumor-infiltrating lymphocytes are associated with Lymphotoxin β-producing dendritic cells in human breast cancer. J. Immunol. 2013; 191:2001–2008. [PubMed: 23825314]
23. Hindley JP, et al. T-cell trafficking facilitated by high endothelial venules is required for tumor control after regulatory T-cell depletion. Cancer Res. 2012; 72:5473–5482. [PubMed: 22962270]
24. Thompson ED, Enriquez HL, Fu Y-X, Engelhard VH. Tumor masses support naive T cell infiltration, activation, and differentiation into effectors. J. Exp. Med. 2010; 207:1791–1804. [PubMed: 20660615]
25. Yu P, et al. Priming of naive T cells inside tumors leads to eradication of established tumors. Nat. Immunol. 2004; 5:141–149. [PubMed: 14704792]
26. Schrama D, et al. Immunological tumor destruction in a murine melanoma model by targeted LTalpha independent of secondary lymphoid tissue. Cancer Immunol. Immunother. 2008; 57:85–95. [PubMed: 17605009]
27. Dankort D, et al. Braf(V600E) cooperates with Pten loss to induce metastatic melanoma. Nat. Genet. 2009; 41:544–552. [PubMed: 19282848]
28. Scimone ML, Aifantis I, Apostolou I, Boehmer H, von & Andrian UH, von. A multistep adhesion cascade for lymphoid progenitor cell homing to the thymus. PNAS. 2006; 103:7006–7011. [PubMed: 16641096]
29. Walch JM, et al. Cognate antigen directs CD8+ T cell migration to vascularized transplants. Journal of Clinical Investigation. 2013; 123:2663–2671. [PubMed: 23676459]
30. Palazón A, et al. Agonist Anti-CD137 mAb Act on Tumor Endothelial Cells to Enhance Recruitment of Activated T Lymphocytes. Cancer Res. 2011; 71:801–811. [PubMed: 21266358]
31. Sasaki K, et al. Preferential expression of very late antigen-4 on type 1 CTL cells plays a critical role in trafficking into central nervous system tumors. Cancer Res. 2007; 67:6451–6458. [PubMed: 17616706]

32. Stein JV, et al. The CC chemokine thymus-derived chemotactic agent 4 (TCA-4, secondary lymphoid tissue chemokine, 6Ckine, exodus-2) triggers lymphocyte function-associated antigen 1-mediated arrest of rolling T lymphocytes in peripheral lymph node high endothelial venules. J. Exp. Med. 2000; 191:61–76. [PubMed: 10620605]
33. Ho P-C, et al. Immune-Based Antitumor Effects of BRAF Inhibitors Rely on Signaling by CD40L and IFNγ. Cancer Res. 2014; 74:3205–3217. [PubMed: 24736544]
34. Damsky WE, et al. β-catenin signaling controls metastasis in Braf-activated Pten-deficient melanomas. Cancer Cell. 2011; 20:741–754. [PubMed: 22172720]
35. Spranger S, Bao R, Gajewski T. Melanoma-intrinsic β-catenin signaling prevents T cell infiltration and anti-tumor immunity. Journal for ImmunoTherapy of Cancer. 2014; 2:O15.
36. Orr MT, Lanier LL. Natural killer cell education and tolerance. Cell. 2010; 142:847–856. [PubMed: 20850008]
37. Shinkai Y, et al. RAG-2-deficient mice lack mature lymphocytes owing to inability to initiate V(D)J rearrangement. Cell. 1992; 68:855–867. [PubMed: 1547487]
38. Fletcher AL, et al. Lymph node fibroblastic reticular cells directly present peripheral tissue antigen under steady-state and inflammatory conditions. J. Exp. Med. 2010; 207:689–97. [PubMed: 20308362]
39. Brinkmann V, et al. The immune modulator FTY720 targets sphingosine 1-phosphate receptors. J. Biol. Chem. 2002; 277:21453–21457. [PubMed: 11967257]
40. Brinkmann V, Lynch KR. FTY720: targeting G-protein-coupled receptors for sphingosine 1-phosphate in transplantation and autoimmunity. Curr. Opin. Immunol. 2002; 14:569–575. [PubMed: 12183155]
41. Sheasley-O'Neill SL, Brinkman CC, Ferguson AR, Dispenza MC, Engelhard VH. Dendritic cell immunization route determines integrin expression and lymphoid and nonlymphoid tissue distribution of CD8 T cells. J. Immunol. 2007; 178:1512–1522. [PubMed: 17237400]
42. Brinkman CC, Sheasley-O'Neill SL, Ferguson AR, Engelhard VH. Activated CD8 T cells redistribute to antigen-free lymph nodes and exhibit effector and memory characteristics. J. Immunol. 2008; 181:1814–1824. [PubMed: 18641319]
43. Cipponi A, et al. Neogenesis of lymphoid structures and antibody responses occur in human melanoma metastases. Cancer Res. 2012; 72:3997–4007. [PubMed: 22850419]
44. Kumar V, et al. Global lymphoid tissue remodeling during a viral infection is orchestrated by a B cell-lymphotoxin-dependent pathway. Blood. 2010; 115:4725–4733. [PubMed: 20185585]
45. Liao S, Ruddle NH. Synchrony of high endothelial venules and lymphatic vessels revealed by immunization. J. Immunol. 2006; 177:3369–3379. [PubMed: 16920978]
46. Furtado GC, et al. Lymphotoxin beta receptor signaling is required for inflammatory lymphangiogenesis in the thyroid. Proc. Natl. Acad. Sci. U.S.A. 2007; 104:5026–5031. [PubMed: 17360402]
47. Kratz A, Campos-Neto A, Hanson MS, Ruddle NH. Chronic Inflammation Caused by Lymphotoxin Is Lymphoid Neogenesis. J. Exp. Med. 1996; 183:1461–1472. [PubMed: 8666904]
48. Sacca R, Cuff CA, Lesslauer W, Ruddle NH. Differential Activities of Secreted Lymphotoxin-α3 and Membrane Lymphotoxin-α1β2 in Lymphotoxin-Induced Inflammation: Critical Role of TNF Receptor 1 Signaling. J. Immunol. 1998; 160:485–491. [PubMed: 9552007]
49. Onder L, et al. Endothelial cell-specific lymphotoxin-β receptor signaling is critical for lymph node and high endothelial venule formation. J. Exp. Med. 2013; 210:465–473. [PubMed: 23420877]
50. Rosen SD. Ligands for L-selectin: homing, inflammation, and beyond. Annu. Rev. Immunol. 2004; 22:129–156. [PubMed: 15032576]
51. Hemmerich S, et al. Sulfation of L-Selectin Ligands by an HEV-Restricted Sulfotransferase Regulates Lymphocyte Homing to Lymph Nodes. Immunity. 2001; 15:237–247. [PubMed: 11520459]
52. Uchimura K, et al. N-Acetylglucosamine 6-O-Sulfotransferase-1 Regulates Expression of L-Selectin Ligands and Lymphocyte Homing. J. Biol. Chem. 2004; 279:35001–35008. [PubMed: 15175329]

53. Kawashima H, et al. N-acetylglucosamine-6-O-sulfotransferases 1 and 2 cooperatively control lymphocyte homing through L-selectin ligand biosynthesis in high endothelial venules. Nat. Immunol. 2005; 6:1096–1104. [PubMed: 16227985]

54. Uchimura K, et al. A major class of L-selectin ligands is eliminated in mice deficient in two sulfotransferases expressed in high endothelial venules. Nat. Immunol. 2005; 6:1105–1113. [PubMed: 16227986]

55. Ngo VN, et al. Lymphotoxin alpha/beta and tumor necrosis factor are required for stromal cell expression of homing chemokines in B and T cell areas of the spleen. J. Exp. Med. 1999; 189:403–412. [PubMed: 9892622]

56. Dejardin E, et al. The Lymphotoxin-β receptor induces different patterns of gene expression via two NF-κB pathways. Immunity. 2002; 17:525–535. [PubMed: 12387745]

57. Hjelmström P, et al. Lymphoid tissue homing chemokines are expressed in chronic inflammation. Am. J. Pathol. 2000; 156:1133–1138. [PubMed: 10751336]

58. Mueller SN, et al. Regulation of homeostatic chemokine expression and cell trafficking during immune responses. Science. 2007; 317:670–674. [PubMed: 17673664]

59. Baekkevold ES, et al. The CCR7 Ligand ELC (CCL19) Is Transcytosed in High Endothelial Venules and Mediates T Cell Recruitment. J. Exp. Med. 2001; 193:1105–1112. [PubMed: 11342595]

60. Berahovich RD, Lai NL, Wei Z, Lanier LL, Schall TJ. Evidence for NK cell subsets based on chemokine receptor expression. J. Immunol. 2006; 177:7833–7840. [PubMed: 17114454]

61. Lanier LL. NK cell recognition. Annu. Rev. Immunol. 2005; 23:225–274. [PubMed: 15771571]

62. Sigmundsdottir H, Butcher EC. Environmental cues, dendritic cells and the programming of tissue-selective lymphocyte trafficking. Nat. Immunol. 2008; 9:981–987. [PubMed: 18711435]

63. Schreiber RD, Hicks LJ, Celada A, Buchmeier NA, Gray PW. Monoclonal antibodies to murine gamma-interferon which differentially modulate macrophage activation and antiviral activity. J. Immunol. 1985; 134:1609–1618. [PubMed: 2578513]

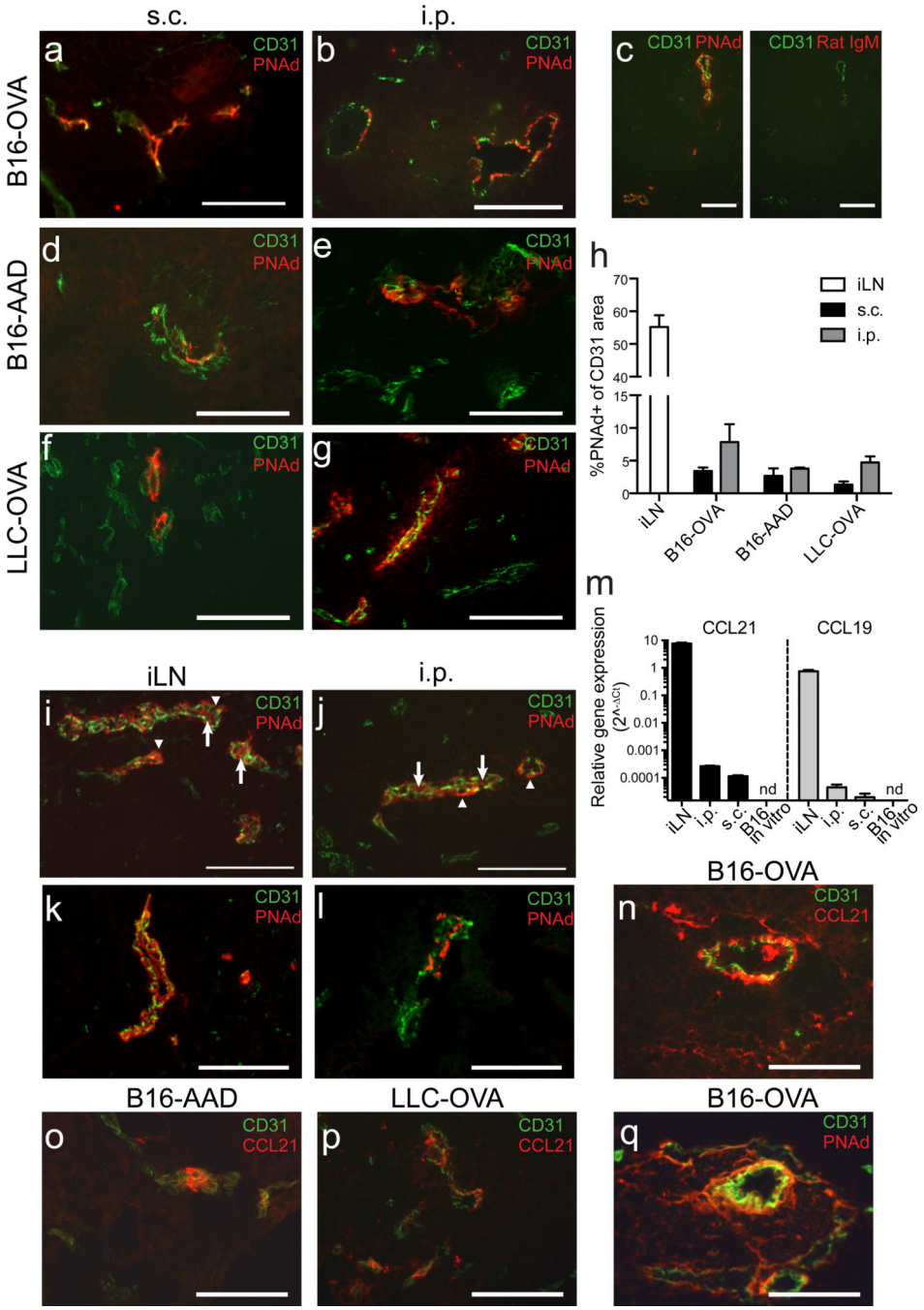

Figure 1. Tumors spontaneously develop LN-like vasculature expressing PNAd and CCL21

(a–g) Frozen sections of d 14 B16-OVA tumors (a–c), B16-AAD tumors (d–e), or LLC-OVA tumors (f–g) growing s.c. (a,d,f) and i.p. (b,c,e,g) in C57BL/6 mice were stained for CD31 and PNAd. In (c) two adjacent sections were stained for CD31 and with either PNAd or Rat IgM isotype control antibody.

(h) The percentage of $CD31^+$ area expressing PNAd in each tissue was quantified as described in Methods. iLN is inguinal LN. Bars represent mean+SEM. n=4 per tissue.

(i–l) PNAd staining on HEV in inguinal LN (i,k) and i.p. B16-OVA tumors (j,l). In (i,j) arrows mark luminal PNAd, arrowheads mark abluminal PNAd. In (k,l) luminal PNAd was detected with streptavidin after i.v. injection of biotinylated MECA-79 antibody 30 m prior to harvest.

(m) Expression of *Ccl21*, *Ccl19* and *Hprt* mRNA in *in vitro* B16-cOVA cultures, and lysates (n=3) of s.c. and i.p. B16-cOVA tumors and inguinal LN was detected using 40-cycle RT-PCR. Relative gene expression is presented as $2^{\wedge}-\Delta C_T$ relative to HPRT.

(n–q) Sections of i.p. B16-OVA tumors (n,q), B16-AAD tumors (o), or LLC-OVA tumors (p) were stained for CD31 and either CCL21 (n–p) or PNAd (q). Two adjacent sections are shown in (n) and (q).

All images are representative of at least 3 independent experiments. Scale bars = 100 μm

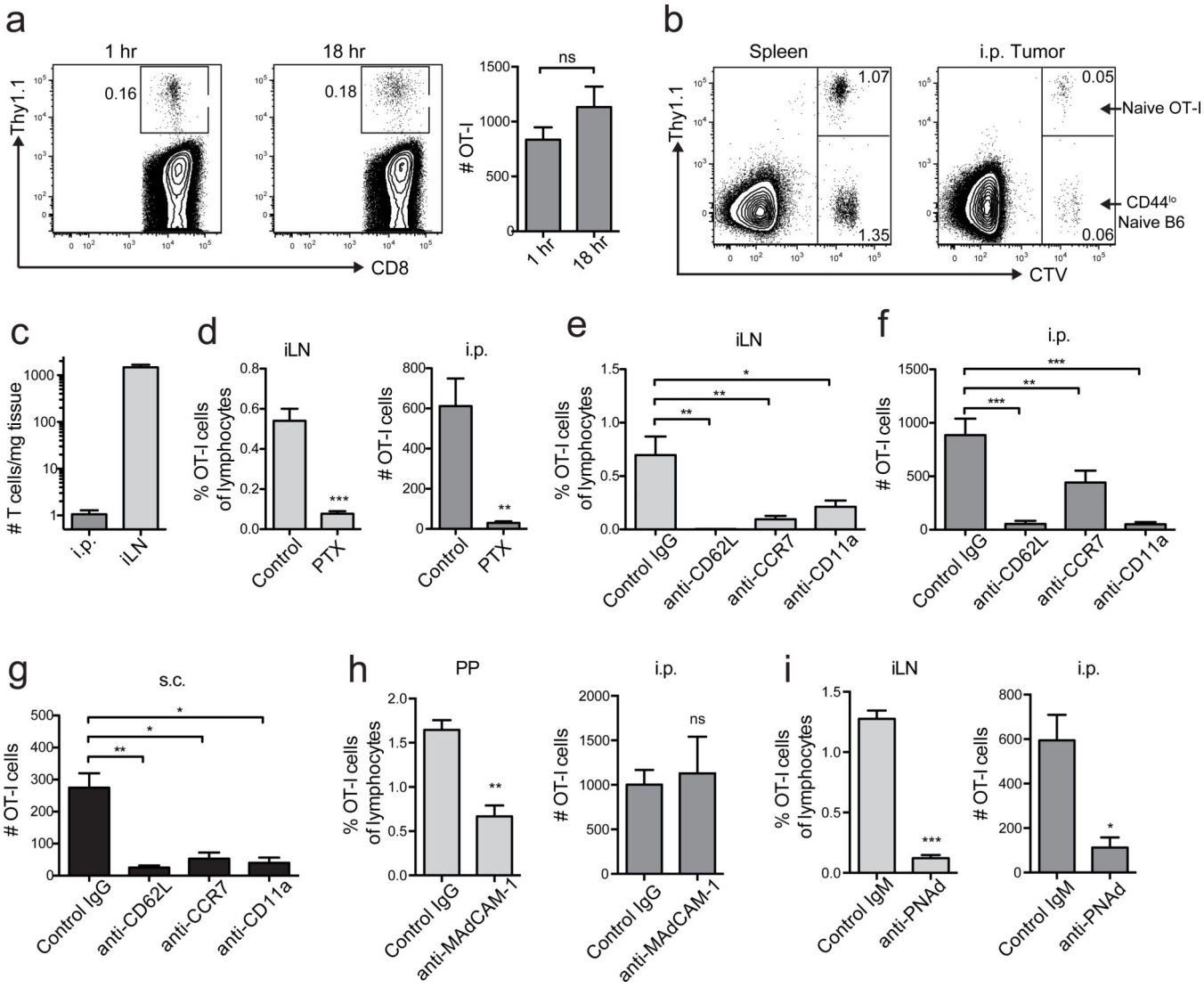

Figure 2. LN-like vasculature supports naïve T-cell infiltration

(a) Representative plots and summary data (n=3) for naïve T-cell infiltration. 4×10^6 naïve Thy1.1$^+$ OT-I cells were injected i.v. into WT mice with established i.p. B16-OVA tumors. 1 h or 18 h after transfer, tumors were harvested, and infiltrating naïve T-cells were enumerated by flow cytometry. Numbers indicate the percentage of naïve OT-I cells out of the live singlet CD45$^+$ CD8$^+$ parent gate.

(b) WT mice with i.p. B16-OVA tumors received a 50:50 mix of CTV-labeled naïve Thy1.1$^+$ OT-I cells and CD44^{lo} naïve T-cells from C57BL/6 mice i.v. (4×10^6 total cells). Infiltration into tissues was determined after 18 h.

(c) Homing efficiency (# T-cells/mg tissue) of naïve OT-I cells to i.p. tumors and inguinal LN. n=7.

(d–g) Naïve OT-I cells pretreated with pertussis toxin (PTX) (d) or antibodies against L-selectin (CD62L), CCR7, or LFA-1 (CD11a) (e–g) were transferred into tumor bearing mice. Infiltration into inguinal LN (d,e), i.p. (d,f) or s.c. (g) B16-OVA tumors was determined after 18 h. n=10–17 per group (tumors) or 4 per group (iLN).

(h,i) Naïve OT-I cells were transferred into WT mice with i.p. B16-OVA tumors pre-treated with anti-MAdCAM-1 antibody or Rat IgG isotype control (h) or anti-PNAd antibody or Rat IgM isotype control (i). Infiltration into tissues was determined 1 h after T-cell transfer. n=5 (h) or 3(i). PP are Peyer's Patches, iLN is inguinal lymph node.

Data (mean+SEM) are pooled from 2 independent experiments. ns:$p>0.05$, *$p<0.05$, **$p<0.01$, ***$p<0.001$ by unpaired t test (a,c,h,i) or one way ANOVA with Dunnett's post-test (e–g).

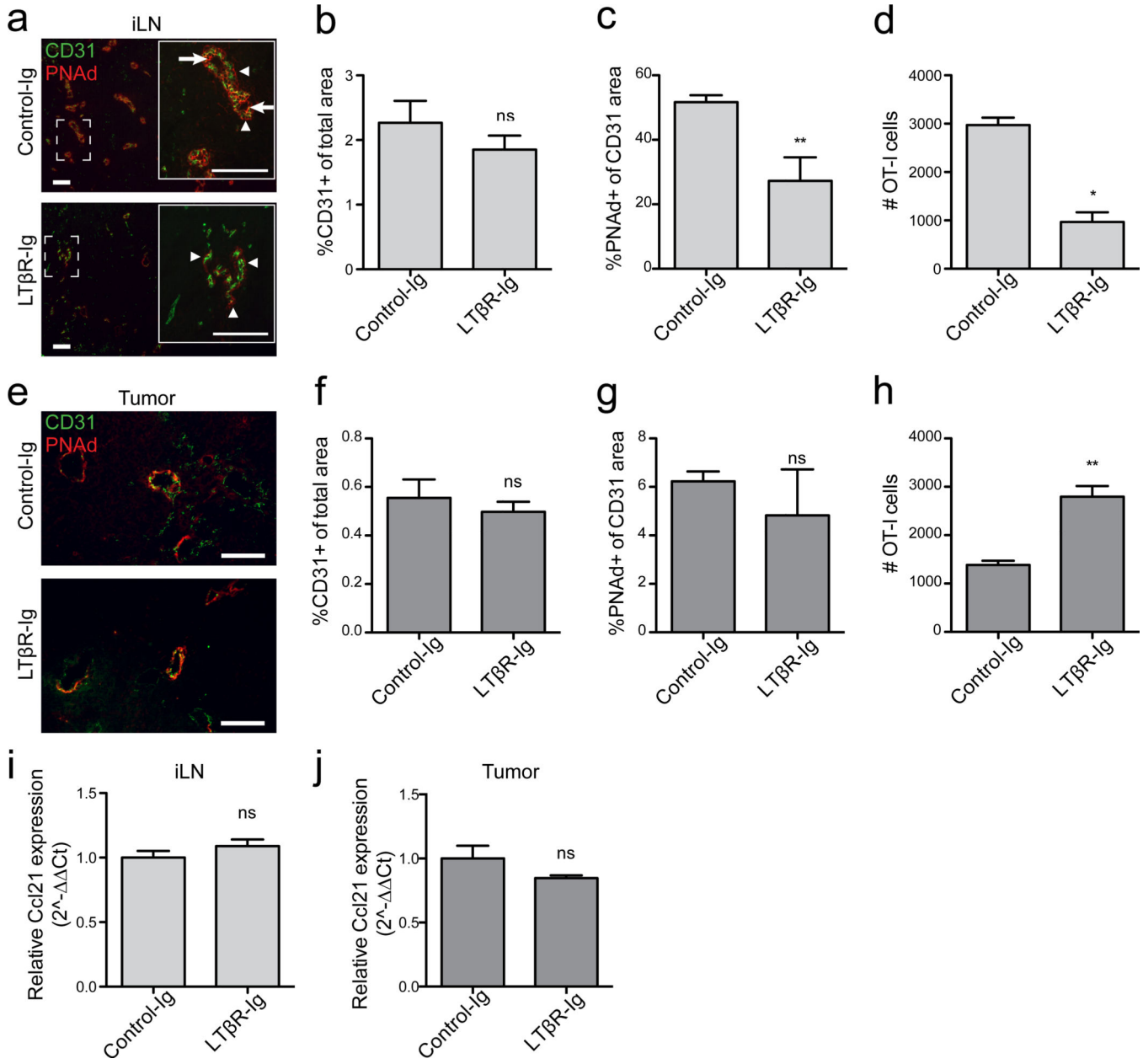

Figure 3. Expression of PNAd and CCL21 in B16-OVA tumors does not require LTβR signaling

(a–c) Expression of CD31 and PNAd in inguinal LN from control-Ig or LTβR-Ig treated mice. (a) Boxed area is shown in inset. Arrows mark luminal PNAd, arrowheads mark abluminal PNAd.

(b,c) Percentages of total area positive for CD31 (b) and of the CD31 area positive for PNAd (c) were calculated as described in Methods. n=4–5 per group (b) or 9–10 per group (c).

(d) Infiltration of naïve OT-I cells into inguinal LN of control-Ig and LTβR-Ig treated mice determined as in Figure 2. n=3.

(e–g) Expression of CD31 and PNAd in i.p. tumors from control-Ig or LTβR-Ig treated mice. Expression was analyzed in mice that did not receive naïve OT-I T-cells. n=5 per group.

(h) Infiltration of naïve OT-I cells into i.p. tumors of control-Ig and LTβR-Ig treated mice. n=5 per group.

(i,j) Expression of *Ccl21* in LN (i) and i.p. tumor (j) lysates was determined by quantitative RT-PCR. Results were calculated by the $\Delta\Delta C_T$ method relative to HPRT with expression levels in control samples normalized to 1. n=≥3 per group

Data (mean+SEM) are representative of two independent experiments. ns:p>0.05, *p<0.05, **p<0.01 by unpaired t-test. Scale bars = 100 μm.

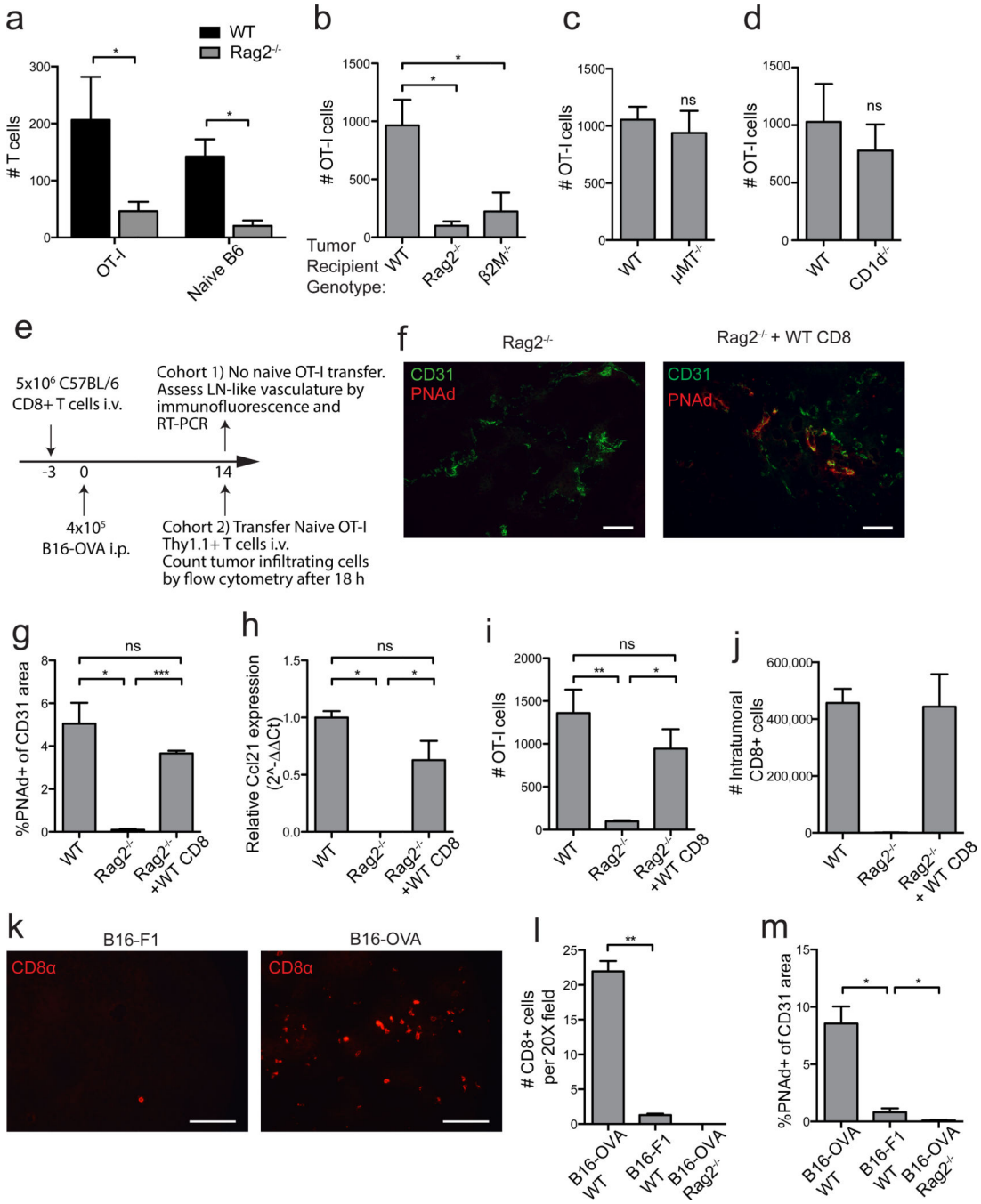

Figure 4. Endogenous CD8 T-cells induce LN-like vasculature in i.p. tumors

(a) Infiltration of naïve Thy1.1^{+} OT-I cells and CD44^{lo} naïve polyclonal T-cells purified from C57BL/6 and co-transferred into WT or *Rag2*$^{-/-}$ mice with established i.p. B16-OVA tumors was determined after 18 h by flow cytometry. n=3 per genotype.

(b–d) Infiltration of naïve OT-I cells into i.p. B16-OVA tumors in the indicated mice was determined. n=3 (b) or 5 (c–d).

(e) Experimental protocol used for the repletion of *Rag2*$^{-/-}$ mice with CD8 T-cells prior to tumor implantation. On d 14 after tumor implantation, tumors from one cohort of mice were

harvested for immunofluorescence and RT-PCR. A second cohort of mice received naïve OT-I cells and tumors were processed for flow cytometry to assess infiltration into tumors.
(f,g) Representative images (f) and summary data (g, n=3–4) for PNAd expression in tumors in the indicated mice.
(h) *Ccl21* expression (n=2) in i.p. tumor lysates was quantified as in Figure 3.
(i) Infiltration of naïve OT-I cells into i.p. B16-OVA tumors in the indicated mice was determined. n=3–5 per group.
(j) The absolute number of endogenous (non-OT-I) $CD8^+$ T-cells that had accumulated in d 14 i.p. B16-OVA tumors in mice with the indicated background was determined by flow cytometry.
(k,l) Representative images (k) and summary data (l, n=2) for endogenous CD8 T-cell accumulation in d 14 B16-F1 or B16-OVA tumors growing in WT mice determined by immunofluorescence.
(m) Expression of PNAd in either B16-F1 or B16-OVA tumors growing in the indicated mice. n=4 per group.
Data (mean+SEM) are representative of at least two independent experiments. ns:$p>0.05$, *$p<0.05$, **$p<0.01$, ***$p<0.001$ by unpaired t-test (a,c,d) or one way ANOVA with Tukey's post-test (b,g-m).

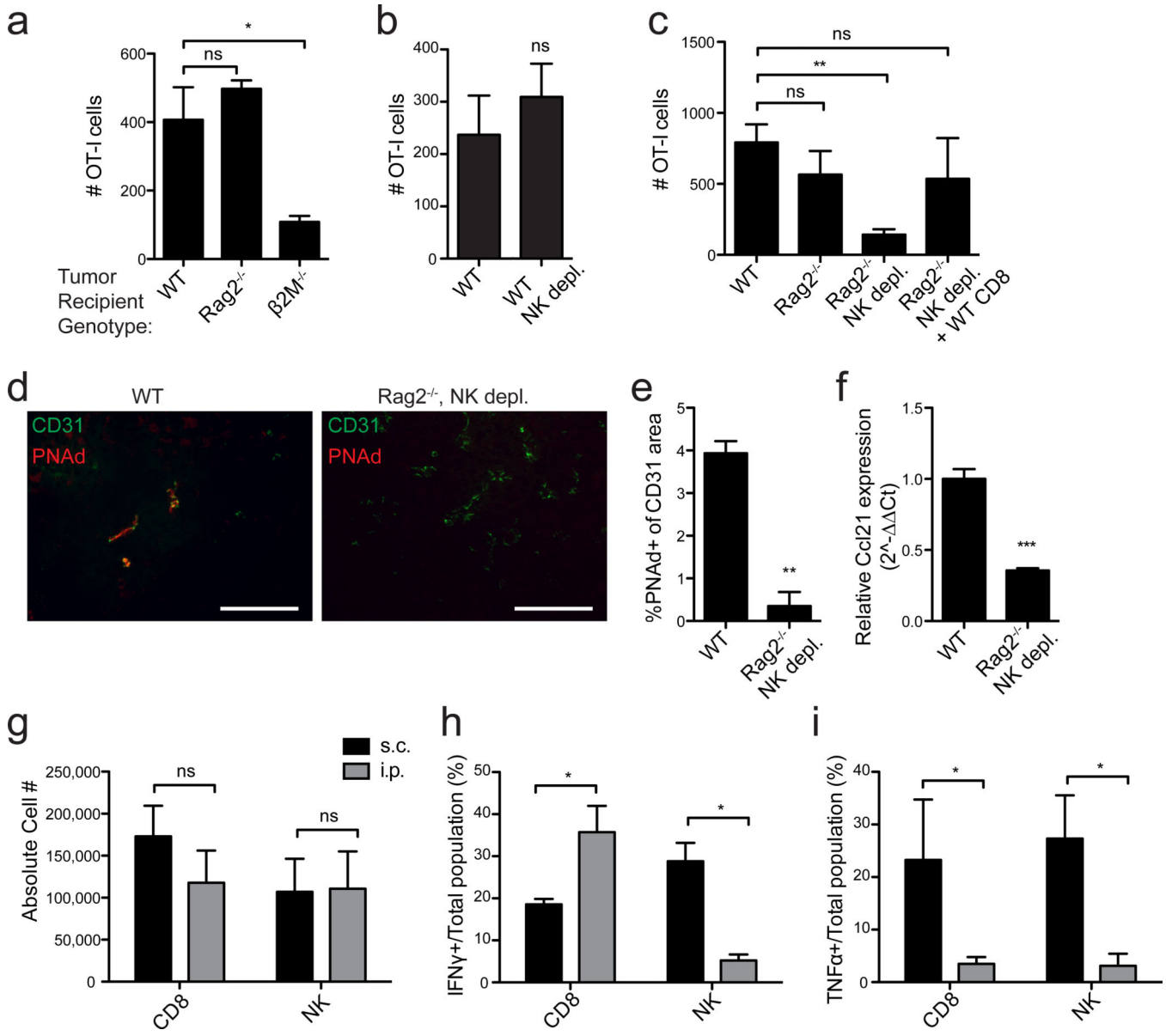

Figure 5. CD8 T-cells and NK cells act redundantly to induce LN-like vasculature in s.c. tumors

(a–c) Infiltration of naïve OT-I cells into s.c. B16-OVA tumors in the indicated mice was determined as in Figure 2. n=3 (a) or 5–8 (b,c) per group.

(d,e) Representative images (d) and summary data (e, n=3) for PNAd expression in tumors in the indicated mice.

(f) *Ccl21* expression (n=3) in s.c. tumor lysates was quantified as in Figure 3.

(g) Number of endogenous CD8 T-cells ($CD3^+CD8^+$) and NK cells ($CD3^-CD4^-NK1.1^+$) present in s.c. (black bars) and i.p. (gray bars) tumors in WT mice was determined by flow cytometry. n≥8 per group.

(h,i) The percentage of total CD8 T-cells or NK cells producing IFNγ (h) or TNFα (i) in s.c. (black bars) or i.p. (gray bars) tumors from WT mice was assessed by intracellular staining 4 hr after Brefeldin A injection. n=3–5 per group

Data (mean+SEM) are representative of at least two independent experiments. ns:$p>0.05$, *$p<0.05$, **$p<0.01$, ***$p<0.001$ by unpaired t-test (b,e-i) or one way ANOVA with Dunnett's post-test (a,c).

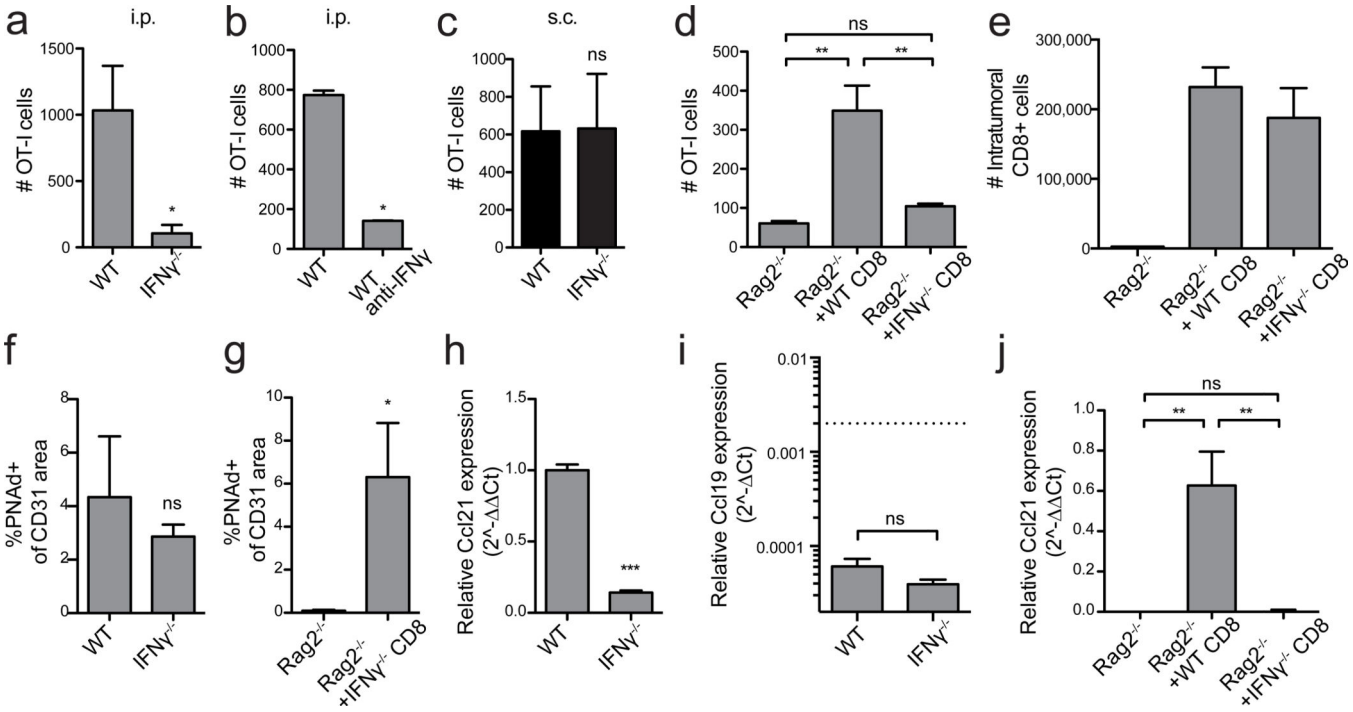

Figure 6. IFNγ from endogenous CD8 T-cells controls CCL21 but not PNAd expression in i.p. tumors

(a–d) Infiltration of naïve OT-I cells into i.p. (a,b,d) or s.c. (c) B16-OVA tumors in the indicated mice was determined as in Figure 2. n=7 (a), 3 (b,d), 5 (c). In (d), *Rag2*$^{-/-}$ mice were repleted with either WT or *IFNγ*$^{-/-}$ CD8 T-cells prior to tumor implantation.

(e) The absolute number of CD8^{+} T-cells (non-OT-I) that had accumulated in i.p. B16-OVA tumors in mice with the indicated background was determined by flow cytometry. n=3 per group.

(f,g) PNAd expression in i.p. tumors from the indicated mice was quantified as in Figure 3. n=3 per group.

(h–j) *Ccl21* (h,j) or *Ccl19* (i) expression in i.p. tumors lysates from the indicated mice was quantified. *Ccl21* data (h,j) is presented as $2^{\wedge}-\Delta\Delta C_T$ method relative to HPRT with expression levels in control samples normalized to 1. *Ccl19* data (i) is presented as $2^{\wedge}-\Delta C_T$ relative to HPRT. Dashed line represents *Ccl21* expression levels in control tumors. n=3–6 per group.

Data (mean+SEM) are representative at least two independent experiments. ns:p>0.05, *p<0.05, **p<0.01, ***p<0.001 by unpaired t-test (a-c,f-h) or one way ANOVA with Tukey's post-test (d,i).

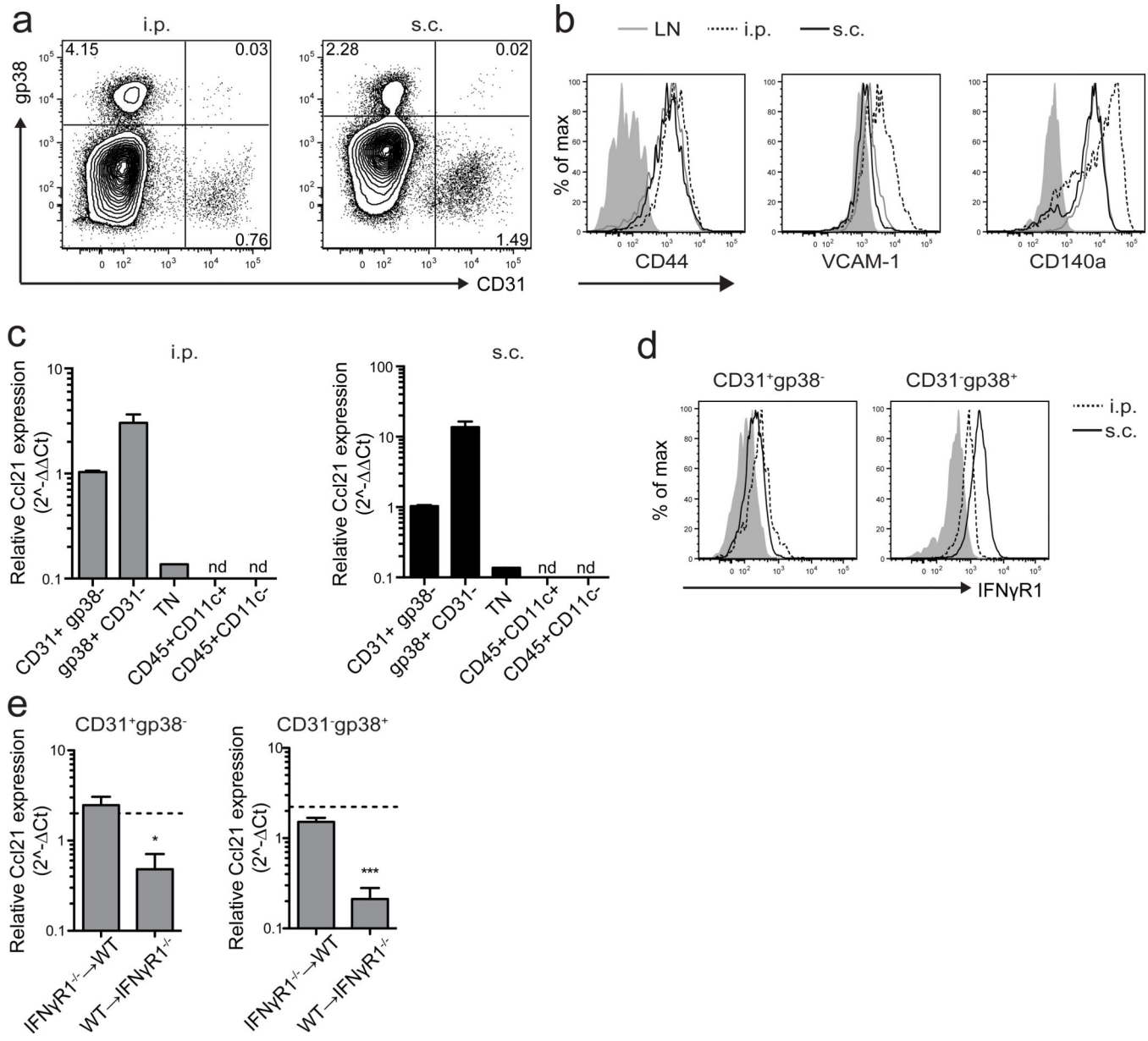

Figure 7. IFNγ controls CCL21 expression by endothelial cells and gp38$^+$ cells

(a) Frequency of gp38$^+$ and CD31$^+$ cells among live singlet Ter119^{neg}CD45^{neg} cells from i.p. and s.c. tumors was determined by flow cytometry.

(b) The phenotype of gp38$^+$ cells from LN (solid gray lines), s.c. (solid black lines) and i.p. (dotted lines) B16-OVA tumors was determined by flow cytometry by staining with the indicated markers. The parent gate is live singlet CD45^{neg} gp38$^+$ CD31^{neg}. Shaded regions represent background staining in FMO controls.

(c) *Ccl21* expression in the indicated purified cell populations from i.p. and s.c. tumors was measured by RT-PCR. Expression levels in CD31$^+$ endothelial cells for each tumor location were normalized to 1. TN = CD45^{neg} gp38^{neg} CD31^{neg}. n=3. nd=not detected.

(d) IFNγR1 expression on $CD31^+$ and $gp38^+$ cells from i.p. (dashed lines) and s.c. (solid lines) tumors was determined by flow cytometry. Shaded regions represent background staining in FMO controls.

(e) *Ccl21* expression in purified cell populations isolated from i.p. tumors in *IFNγR1−/−➔WT* and *WT➔IFNγR1−/−* bone marrow chimeras was measured by RT-PCR. Expression levels are presented relative to *Hprt*. Dashed lines represent expression levels in WT➔WT control chimera. n=4 per group.

Data (mean+SEM) are representative of three (a–d) independent experiments or one experiment (e). ns:$p>0.05$, *$p<0.05$, ***$p<0.001$ by unpaired t-test.

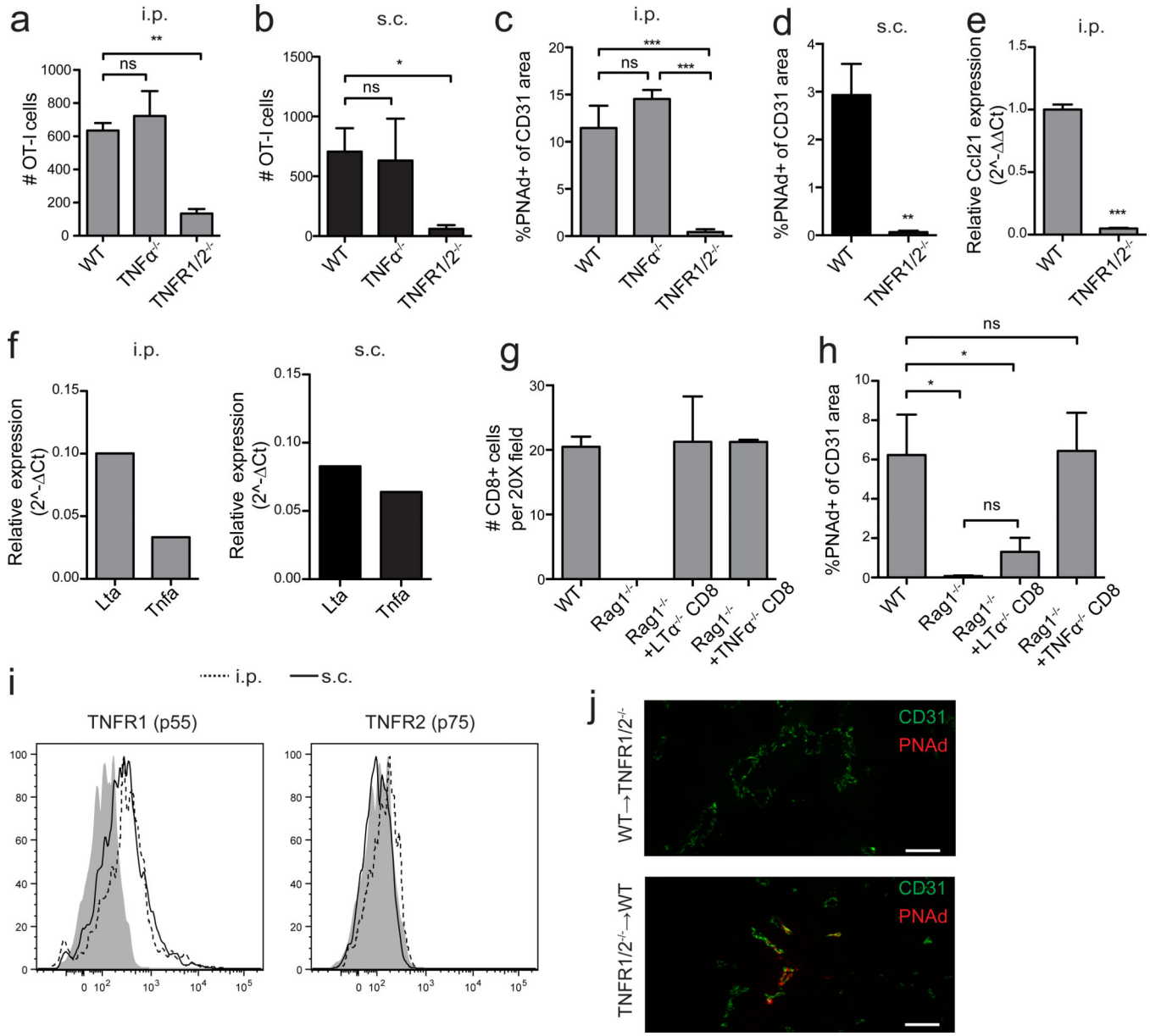

Figure 8. LTα$_3$ induces PNAd expression on tumor vasculature by signaling through TNF receptors

(a,b) Infiltration of naïve OT-I cells into i.p. (a) or s.c. (b) B16-OVA tumors in the indicated mice was determined. n=7 (a) or 4 (b) per group.

(c–e) PNAd expression (c,d) and *Ccl21* expression in i.p. (c,e) or s.c. (d) tumors was quantified. n=4 per group.

(f) Expression of *Lta* and *Tnfa* mRNA in sorted CD3$^+$CD8$^+$ T-cells from i.p. (left panel) and s.c. (right panel) tumors was determined by quantitative RT-PCR. Expression levels are displayed relative to *Hprt*.

(g) Endogenous CD8 T-cell accumulation in d 14 i.p. B16-OVA tumors growing in WT, *Rag1*$^{-/-}$, and *Rag1*$^{-/-}$ mice repleted with either *TNFα*$^{-/-}$ or *LTα*$^{-/-}$ CD8 T-cells mice (n=3 per group) was determined by immunofluorescence.

(h) PNAd expression in i.p. tumors from the indicated mice was determined. n=4 per group.
(i) Expression of TNFR1 and TNFR2 on $CD31^+$ endothelial cells from i.p. (dashed lines) and s.c. (solid lines) B16-OVA tumors was determined by flow cytometry. Shaded region represents background staining in FMO controls.
(j) CD31 and PNAd expression in i.p. tumors from *WT➔TNFR1/2*$^{-/-}$ or *TNFR1/2*$^{-/-}$*➔WT* bone marrow chimeras.
Data (mean+SEM) are pooled from two experiments (a,b) or representative of two (c–j) independent experiments. ns:p>0.05, *p<0.05, **p<0.01, ***p<0.001 by unpaired t-test (d–e) or one way ANOVA with Tukey's post-test (a-c,h). Scale bars = 100 μm.

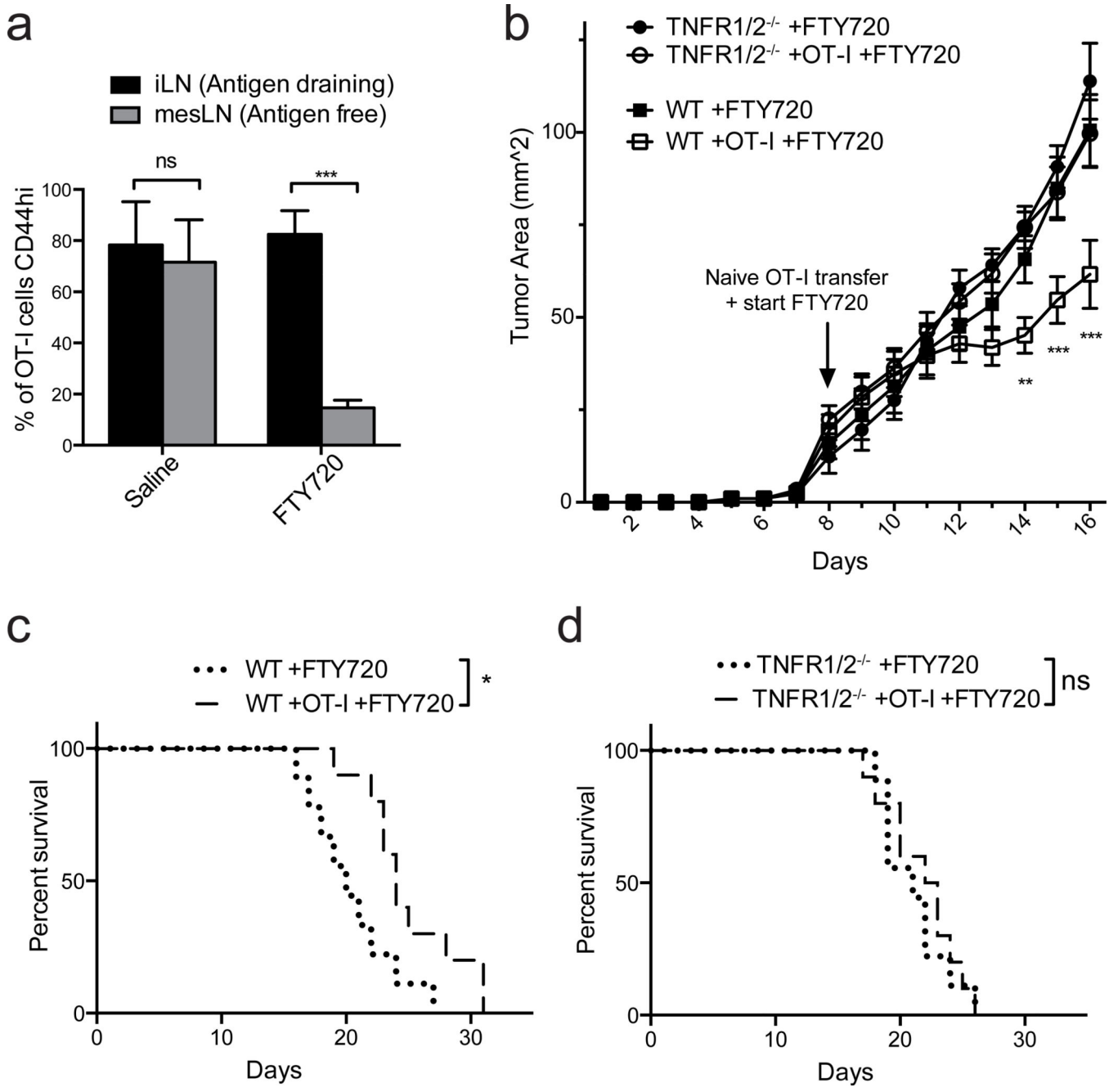

Figure 9. Naïve CD8 T-cells that infiltrate tumors via LN-like vasculature delay tumor outgrowth

(a) WT mice with flank s.c. B16-OVA tumors received naïve OT-I cells i.v. on d 8 after tumor implantation, and were given daily i.p. injections of either 1 mg/kg FTY720 or saline beginning at the time of OT-I transfer. Draining inguinal LN (black bars) and non-draining mesenteric LN (grey bars) were harvested when tumors reached size limits. The percentage of OT-I cells expressing CD44 was determined by flow cytometry. n=5 per group.

(b) WT or *TNFR1/2*$^{-/-}$ mice were implanted s.c. with B16-OVA tumors and received naïve OT-I cells or no T-cells on d 8 after tumor implantation. All mice were treated daily with

FTY720 beginning on d 8. Tumor size was monitored daily by caliper measurements, and tumor area (b) and survival (c,d) was determined. n=9 (no OT-I T cells) or 10 (OT-I T cells). Data (mean+SEM) are representative of two independent experiments. ns:$p>0.05$, *$p<0.05$, **$p<0.01$, ***$p<0.001$ by unpaired t-test (a), two way ANOVA (b) or Log-rank test (c,d).

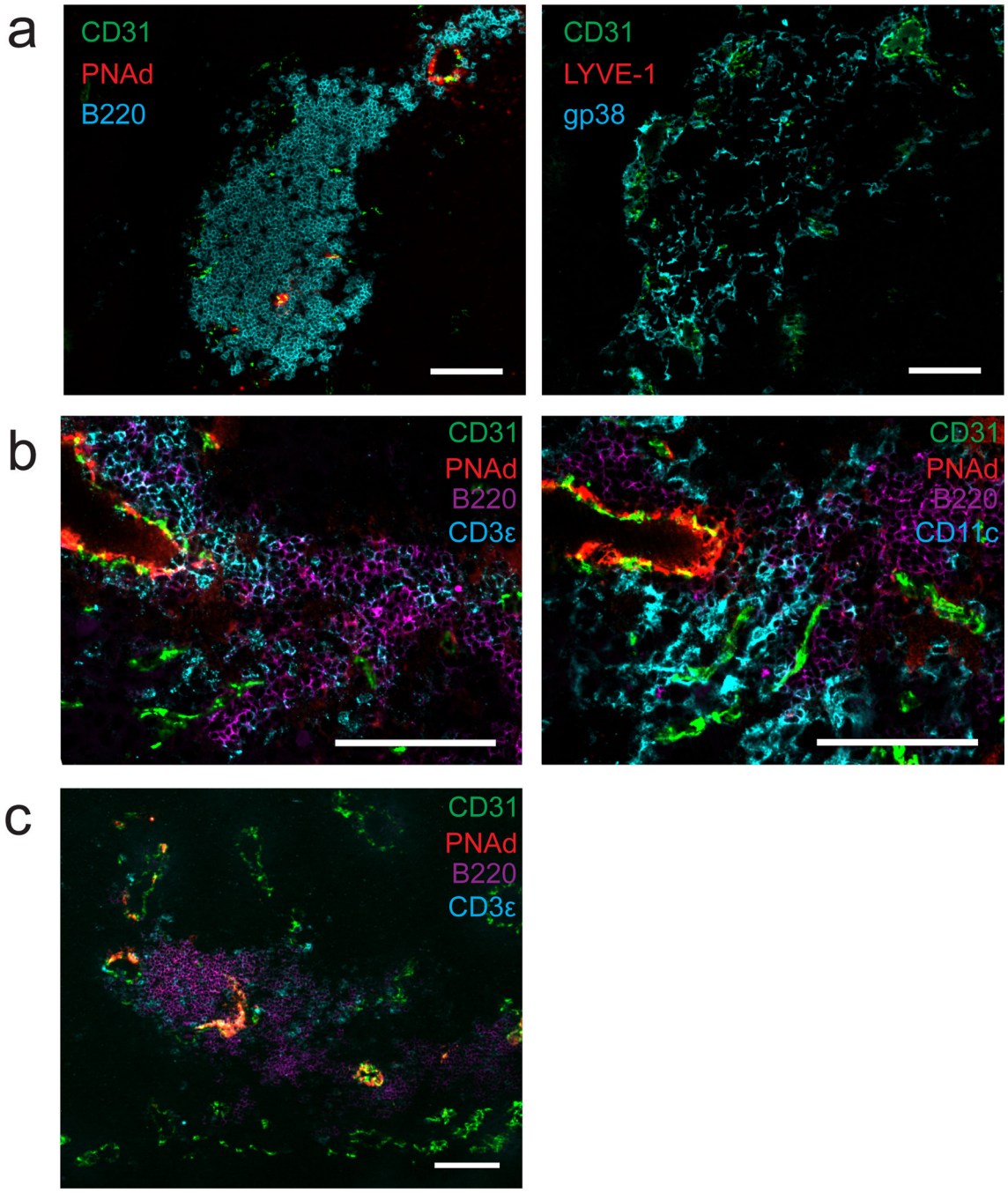

Figure 10. LN-like vasculature is associated with organized lymphoid tissue in i.p. B16-OVA tumors

(a–c) i.p. B16-OVA tumors from C57BL/6 mice stained for the indicated cellular markers. Two adjacent sections were stained in (a). Two different adjacent sections were stained in (b). Images are representative of 5 tumors. Scale bars = 100 μm.